A pentadentate member of the picolinate family for Mn(II) complexation and an amphiphilic derivative[i]

Rosa Pujales-Paradela[a], Fabio Carniato[b], Rocío Uzal-Varela[a], Isabel Brandariz[a], Emilia Iglesias[a], Carlos Platas-Iglesias[a], Mauro Botta[b*] and David Esteban-Gómez[a†]

[a] Universidade da Coruña, Centro de Investigacións Científicas Avanzadas (CICA) and Departamento de Química, Facultade de Ciencias, A Coruña, Galicia, Spain

[b] Dipartimento di Scienze e Innovazione Tecnologica, Università del Piemonte Orientale "A. Avogadro", Viale T. Michel 11, 15121 Alessandria, Italy

Dalton Transactions, volume 48, issue 2, pages 696–710, 14 January 2019
Submitted 24 September 2018, accepted 3 December 2018, first published 04 December 2018

How to cite:

R. Pujales-Paradela, F. Carniato, R. Uzal-Varela, I. Brandariz, E. Iglesias, C. Platas-Iglesias, M. Botta and D. Esteban-Gómez, A pentadentate member of the picolinate family for Mn(II) complexation and an amphiphilic derivative, *Dalt. Trans.*, 2019, **48**, 696–710. DOI: 10.1039/C8DT03856B.

Abstract

We report a pentadentate ligand containing a 2,2′-azanediyldiacetic acid moiety functionalized with a picolinate group at the nitrogen atom (H_3paada), as well as a lipophylic derivative functionalized with a dodecyloxy group at position 4 of the pyridyl ring (H_3C_{12}Opaada). The protonation constants of the paada^{3-} ligand and the stability constant of the Mn(II) complex were determined using a combination of potentiometric and spectrophotometric titrations (25 °C, 0.15 M NaCl). A detailed relaxometric characterisation was accomplished by recording ^{1}H Nuclear Magnetic Relaxation Dispersion (NMRD) profiles and ^{17}O chemical shifts and relaxation rates. These studies provide detailed information on the microscopic parameters that control their efficiency as relaxation agents *in vitro*. For the sake of completeness and to facilitate comparison, we also characterised the related [Mn(nta)]$^-$ complex (nta = nitrilotriacetate). Both the [Mn(paada)]$^-$ and [Mn(nta)]$^-$ complexes turned out to contain two inner-sphere water molecules in aqueous solution. The exchange rate of these coordinated water molecules was slower in [Mn(paada)]$^-$ (k^{298}_{ex} = 90 × 10^7 s^{-1}) than in [Mn(nta)]$^-$ (k^{298}_{ex} = 280 × 10^7 s^{-1}). The complexes were also characterised using both DFT (TPSSh/def2–TZVP) and *ab initio* CAS(5,5) calculations. The lipophylic [Mn(C_{12}Opaada)]$^-$ complex forms micelles in solution characterised by a critical micellar concentration (*cmc*) of 0.31 ± 0.01 mM. This complex also forms a rather strong adduct with Bovine Serum Albumin (BSA) with an association constant of 5.5 × 10^4 M^{-1} at 25 °C. The enthalpy and entropy changes obtained for the formation of the adduct indicate that the binding event is driven by hydrophobic interactions.

Introduction

Acyclic polydentate ligands containing picolinate groups have been intensively investigated in the last decade due to their ability to form stable complexes with a wide range of metal ions. The most common

* mauro.botta@uniupo.it
† david.esteban@udc.es

examples of this ligand class contain a number of amine nitrogen atoms ranging from 1 to 3 functionalised with several 6-methylpicolinate and acetate pendant arms. A judicious choice of the number and type of donor atoms provided ligands with denticity ranging from 5 (*i.e.* dpaMea^{2-})[1] to 10 (*i.e.* decapa^{5-} or tpaen^{4-}, Scheme 1).[2,3] The hexadentate ligand dedpa^{2-} and the rigidified derivative *CHX*dedpa^{2-} and lipophilic derivatives were found to be particularly well suited for the complexation of small metal ions relevant in radiopharmaceutical applications, such as Ga(III) and Cu(II),[4,5] as well as Zn(II), Cd(II) and Pb(II).[6] The Ni(II) complexes with the bis-amide derivatives dedpam and *CHX*dedpam were recently investigated as potential contrast agents for application in Magnetic Resonance Imaging (MRI) based on the Chemical Exchange Saturation Transfer (CEST) effect.[7] Another versatile hexadentate ligand is dpaa^{3-}, which was shown to present favourable Ga^{3+} complexation kinetics giving a rather stable complex.[8] The Mn(II) complex was proposed as a potential alternative to Gd^{3+} as contrast agent for application in MRI thanks to the presence of one water molecule directly coordinated to the metal ion.[9,10] The octadentate ligand octapa^{4-} was demonstrated to form stable complexes with larger metal ions such as In^{3+} and the lanthanide ions (Ln^{3+}).[2,11] As a result, octapa^{4-} and the rigidified derivative *CHX*octapa^{4-} were proposed as chelators for the preparation of ^{111}In and ^{177}Lu radiopharmaceuticals[5] and potential Gd^{3+}–based contrast agents for application in MRI.[12] The pentadentate ligand pmpa^{2-} was also proposed recently as a potential MRI contrast agent endowed with high relaxivity thanks to the presence of two coordinated water molecules.[13]

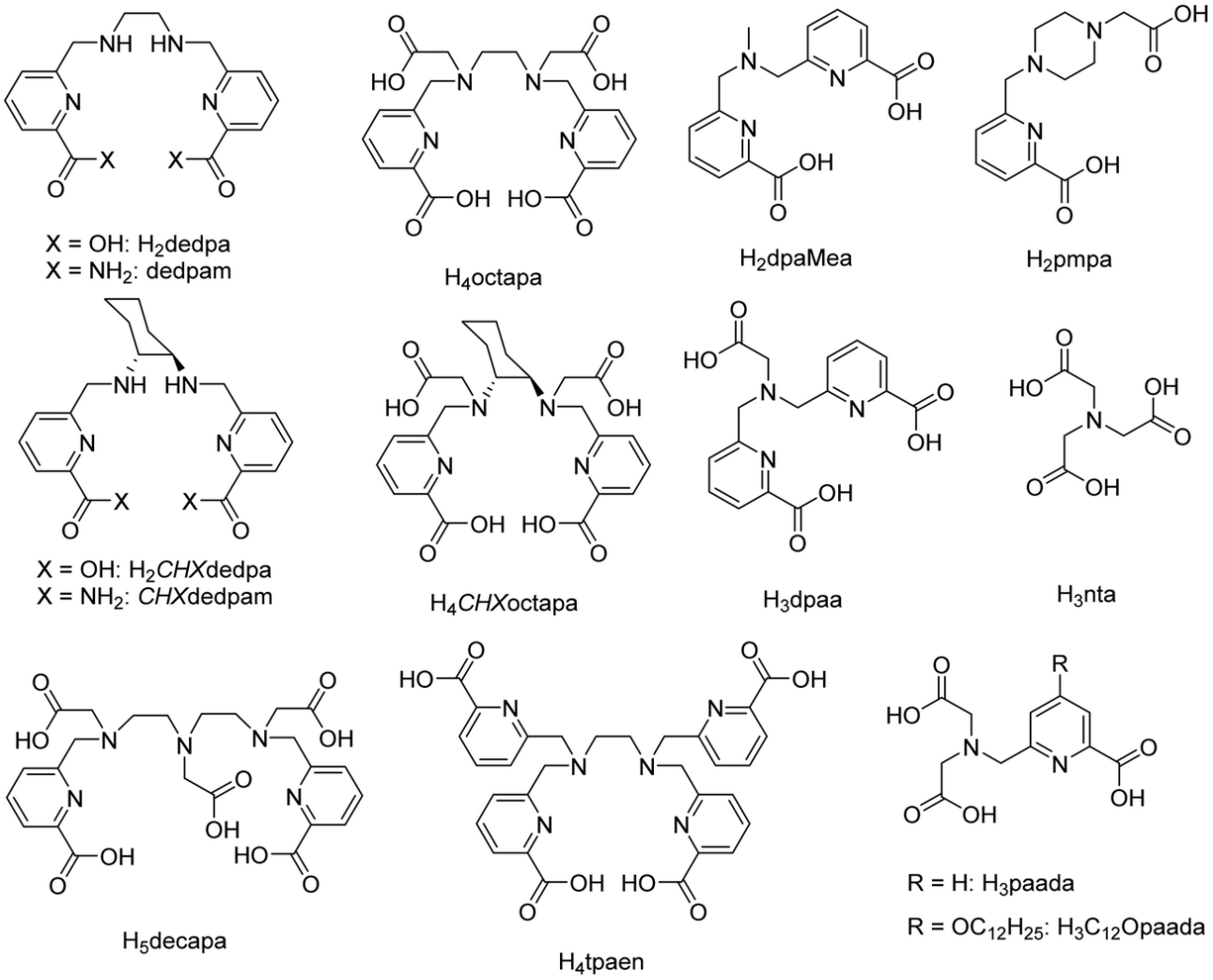

Scheme 1. Structures of the ligands discussed in this work.

Recently we started a research program aiming to develop Mn(II)–based contrast agents for application in MRI. A potential advantage of Mn(II)–based contrast agents with respect to the Gd^{3+} analogues used in clinical practice is related to the better toxicity profile of Mn(II) compared to Gd^{3+}.[14,15] Currently, the issue of Gd^{3+} toxicity is generating some concerns on the use of non-macrocyclic complexes of this metal ion as CAs, particularly in case of administration of multiple doses.[16] Indeed, recent studies also reported Gd^{3+} deposition in the brain and other tissues following the administration of contrast agents.[17] Thus, there is a need for developing safer contrast agent for MRI. High–spin Mn(II) complexes represent an attractive alternative for this purpose, as the d^5 configuration of the metal ion results in slow relaxation times of the electron spin.[18,19] Furthermore, ligands stabilizing both Mn(II) and Mn^{3+} can be used as redox-responsive MRI probes.[20]

In a recent work we investigated the Mn(II) complexes of the pentadentate ligand $dpaMea^{2-}$ and several derivatives containing lipophilic units or multiple $dpaMea^{2-}$ chelating units.[1,9] These complexes feature two water molecules coordinated to the metal ion and present high relaxivities both in aqueous solution and in plasma, where they reversibly bind to human serum albumin (HSA). The incorporation of an acetate arm into the structure of $dpaMea^{2-}$ decreases the number of water molecules coordinated to Mn(II) from 2 to 1, but results in an enhanced thermodynamic stability.[9] Herein, we complete this family of ligands by reporting the pentadentate ligand $paada^{3-}$. This ligand was prepared by Cameron *et al.* and used for complexation of Ru(III) in the search for nitric oxide scavengers.[21] A derivative of $paada^{3-}$ containing a 4-ethynyl-*N*,*N*-dimethyl aniline group at position 4 of the pyridine unit was also developed for complexation of the lanthanide ions.[22] We report in this work an improved synthesis of the ligand. The thermodynamic stability of the corresponding Mn(II) complex was investigated by using potentiometric titrations. A full ^1H and ^{17}O NMR relaxometric characterisation of the complex was carried out to determine the parameters that control the relaxivity of the $[Mn(paada)]^-$ complex. For the sake of comparison, we have also performed a relaxometric study of the related $[Mn(nta)]^-$ complex. Finally, we have synthesised and characterised a lipophilic derivative of $paada^{3-}$ that contains a dodecyloxo group in position 4 of the pyridyl unit ($H_3C_{12}Opaada$, Scheme 1). The ability of this lipophilic derivative to form micelles and bind to BSA was investigated by using relaxometric and spectrofluorometric methods.

Results and discussion

Synthesis of the ligands

A synthesis of H_3paada with a 29% yield was reported in the literature, which involved the alkylation of dimethyl 2,2′-azanediyldiacetate with methyl 6-(((methylsulfonyl)oxy)methyl)picolinate and subsequent basic hydrolysis of the methyl ester groups.[21] The synthesis of H_3paada reported here (Scheme 2) was achieved by alkylation of di-*tert*-butyl 2,2′-azanediyldiacetate with ethyl 6-(chloromethyl)picolinate (**4**) in acetonitrile using K_2CO_3 as a base. Subsequent hydrolysis of the ester groups using 6 M HCl provided H_3paada as its hydrochloride salt with good overall yield (61%).

The synthesis of the lipophilic derivative $H_3C_{12}Opaada$ started from diethyl 4-hydroxy-2,6-pyridinedicarboxylate, which was converted into diethyl 4-dodecyloxy-2,6-pyridinedicarboxylate (**1**) following the literature procedure (Scheme 2).[23] Reduction of one of the ethyl ester groups of **1** with $NaBH_4$ in methanol afforded compound **2**, which was subsequently treated with thionyl chloride to give **3**. Reaction of **3** with di-*tert*-butyl 2,2′-azanediyldiacetate in acetonitrile using K_2CO_3 as a base followed by acid hydrolysis of the ester groups provided the $H_3C_{12}Opaada$ ligand.

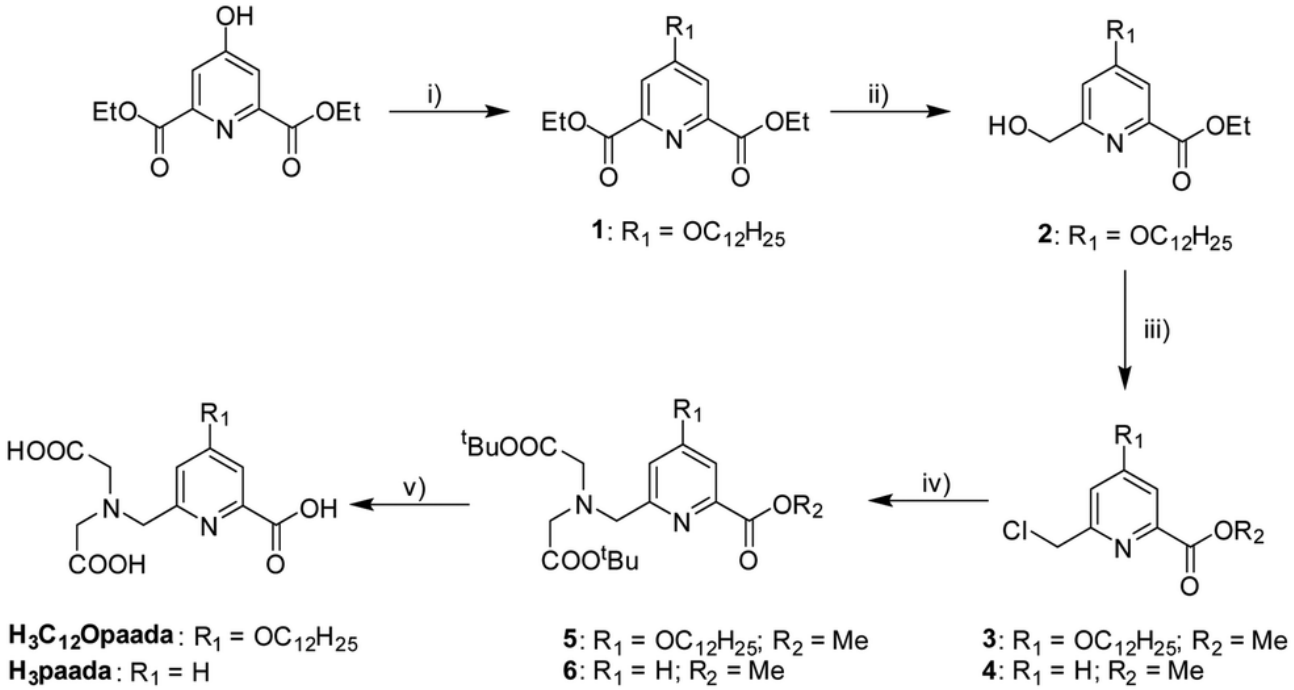

Scheme 2. Synthesis of the ligands. (i) K_2CO_3, $C_{12}H_{25}Br$, acetonitrile; (ii) $NaBH_4$, MeOH; (iii) $SOCl_2$; (iv) K_2CO_3, $(^tBuOOCCH_2)_2NH$, acetonitrile; (v) 6 M HCl, reflux.

Ligand protonation constants and stability constants of the Mn(II) complex

The protonation constants of the paada^{3-} ligand defined as in eqn (1) were determined by potentiometric titrations in 0.15 M NaCl.

$$K_i^{\mathrm{H}} = \frac{[\mathrm{H}_i\mathrm{L}]}{[\mathrm{H}_{i-1}\mathrm{L}][\mathrm{H}^+]} \quad \text{with } i = 1, 2, 3, 4 \qquad (1)$$

The $\log K^{\mathrm{H}}_{\mathrm{i}}$ values determined for paada^{3-} are compared to those of the related dpaMea^{2-}, dpaa^{3-} and nta^{3-} ligands in Table 1. The four protonation constants determined for paada^{3-} are related to the stepwise protonation of the amine nitrogen atom and all the three carboxylate groups of the ligand. The first protonation constant of paada^{3-} is slightly higher than those of dpaa^{3-} and dpaMea^{2-}, but lower than that reported for nta^{3-}. Thus, the amine nitrogen atom of the ligand experiences a decreased basicity upon replacing acetate arms of nta^{3-} by picolinate pendants, an effect that is well documented.[25,26] The second protonation constants of the ligands containing picolinate groups are one log K unit higher than that of nta^{3-}, which indicates that pyridylcarboxylate groups are more prone to protonate than acetate groups.[27] This effect can also be noticed when compared the $\log K^{\mathrm{H}}_3$ values determined for dpaa^{3-} ($\log K^{\mathrm{H}}_3$ = 3.29) and paada^{3-} ($\log K^{\mathrm{H}}_3$ = 2.34). The paada^{3-} ligand presents an overall basicity ($\sum \log K^{\mathrm{H}}_{\mathrm{i}}$, i = 1–4) intermediate between nta^{3-} and dpaa^{3-}.

Table 1. Ligand protonation constants and stability and protonation constants of the corresponding Mn(II) complexes determined using potentiometric titrations (25 °C, 0.15 M NaCl).

	paada^{3-}	dpaa^{3-a}	dpaMea^{2-b}	nta^{3-c}
$\log K_1^{\mathrm{H}}$	8.058(2)	7.26	7.82	9.71
$\log K_2^{\mathrm{H}}$	3.462(4)	3.90	3.71	2.49
$\log K_3^{\mathrm{H}}$	2.34(2)	3.29	2.61	1.86
$\log K_4^{\mathrm{H}}$	1.79(9)	1.77		0.8
$\sum \log K_i^{\mathrm{H}}$	15.65	16.22	14.14	14.86
$\log K_{\mathrm{MnL}}$	9.59(6)	13.19	10.13	7.44
$\log K_{\mathrm{MnLH}}$	2.9(1)[e]/3.1[f]/3.0[g]	2.90	2.57	
pMn[d]	6.93	8.98	7.28	5.21

[a] Data from ref. 9. [b] Data from ref. 1*b*. [c] Data in 0.1 M KCl and 20 °C from ref. 24. [d] Defined as $-\log[\mathrm{Mn}]_{\mathrm{free}}$ with pH = 7.4, [Mn(II)] = [L] = 10^{-5} M. [e] From potentiometric titrations using a 1 : 1 stoichiometry. [f] From potentiometric titrations using a ten-fold excess of Mn(II). [g] From spectrophotometric titrations using a 30-fold excess of Mn(II).

The stability of the Mn(II) complex of paada^{3-} was investigated by using a combination of potentiometric and spectrophotometric experiments at 25 °C in 0.15 M NaCl. The stability constant and protonation constant of the complex are defined in eqn (2) and (3):

$$K_{\mathrm{MnL}} = \frac{[\mathrm{MnL}]}{[\mathrm{Mn}][\mathrm{L}]} \tag{2}$$

$$K_{\mathrm{MnHL}} = \frac{[\mathrm{MnHL}]}{[\mathrm{MnL}][\mathrm{H}^+]} \tag{3}$$

The potentiometric titration data obtained using a 1 : 1 (Mn(II) : H_3paada) ratio could be fitted to a model assuming the formation of a single complex species $[\mathrm{Mn(paada)}]^-$, but the quality of the fit improved when including the protonated complex [Mn(Hpaada)]. To validate the equilibrium model, we carried out potentiometric pH titrations using a ten-fold excess of Mn(II) (1.6×10^{-2} M) with respect to the ligand (1.6×10^{-3} M). Under these conditions, the concentration of [Mn(Hpaada)] at equilibrium increases with respect to the free ligand, whose concentration remains very low. The analysis of the data provided $\log K_{\mathrm{MnHL}} = 3.1$, in good agreement with the value obtained from the titrations performed using 1 : 1 stoichiometry (Table 1).

The formation of a protonated complex species at low pH was further investigated using spectrophotometric experiments. In these experiments a mild acidic solution of the ligand (pH ~ 4, 1.7×10^{-4} M) in the presence of an excess of Mn(II) (5.4×10^{-3} M) was acidified with a standard HCl solution or using trichloroacetic acid as a buffer. In these conditions the main species in solution is the $[\mathrm{Mn(paada)}]^-$ complex, which is transformed into the protonated form as the pH decreases (Fig. 1). This is causing significant changes in the absorption band due to the picolinate chromophore at 272 nm, with the absorbance at the maximum of the

band increasing with decreasing pH. The analysis of the data gives a protonation constant of log K_{MnHL} = 3.0, a value that increases to 3.2 in the presence of buffer. These values are in excellent mutual agreement and match well the potentiometric results.

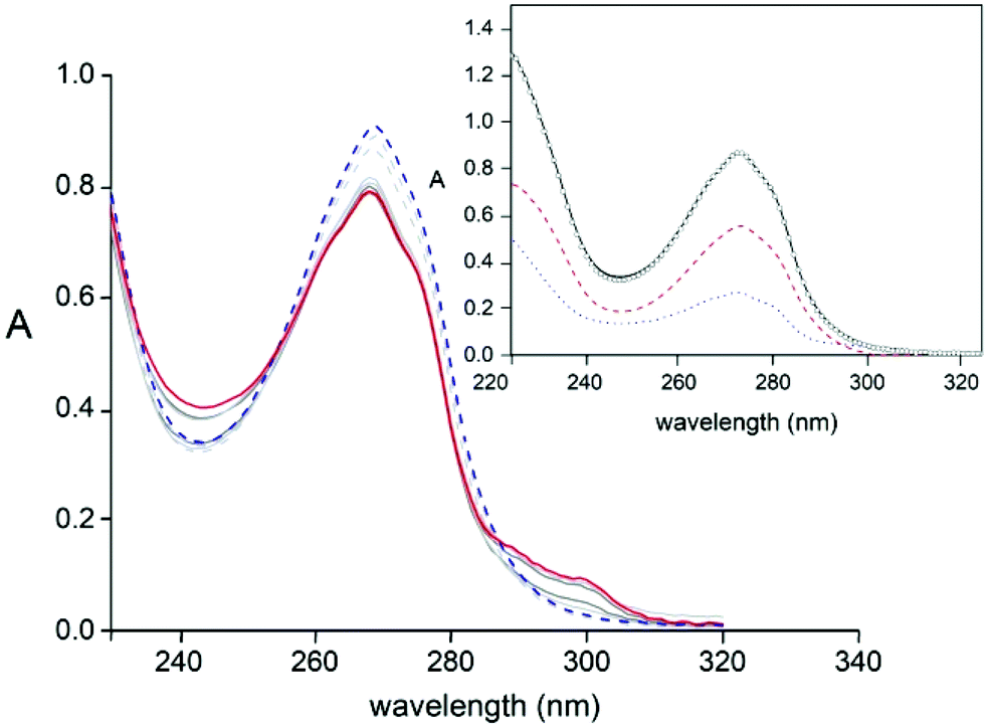

Fig. 1. Absorption spectra of H_3paada (1.7×10^{-4} M) in the presence of an excess of Mn(II) (5.4×10^{-3} M) at different proton concentrations; pH varies from 4 (solid red line) to 2.2 (blue dashed line). Inset: Data at pH = 2.6, the open circles are the experimental points, and the lines are the calculated absorbance values: the solid line is the total absorbance, the dashed line is the absorbance of [Mn(Hpaada)] (58% of the total ligand concentration) and the dotted line is the absorbance of [Mn(paada)$^-$] (35%).

The stability constant of the [Mn(paada)]$^-$ complex lies between those of [Mn(nta)]$^-$ and [Mn(dpaa)]$^-$, reflecting and intermediate denticity of paada^{3-} with respect to tetradentate nta^{3-} and hexadentate dpaa^{3-}. However, the stability of [Mn(paada)]$^-$ is also slightly lower than that of [Mn(dpaMea)], in spite of the lower negative charge of the ligand. These results indicate that the 6,6′-(azanediylbis(methylene))dipicolinate unit present in dpaMea^{2-} and dpaa^{3-} is better suited for the coordination to Mn(II). The thermodynamic stabilities of complexes with different ligands are more appropriately assessed by the pMn values (pMn = $-\log[Mn(II)]_{free}$) defined using the conditions suggested by Drahos[28] (pH = 7.4, [Mn(II)] = [L] = 10^{-5} M). The pMn values follow the same trend observed for the stability constants, with the stability of the complexes decreasing in the order dpaa^{3-} > dpaMea^{2-} > paada^{3-} > nta^{3-} (Table 1). The pMn value calculated for the approved contrast agent mangafodipir trisodium (Na_3[Mn(dpdp)], TELASCAN®, pMn = 7.2)[29] is only slightly higher than that of the dpaa^{3-} complex. These pMn values are nevertheless considerably lower than that of [Mn(paada)]$^-$ (pMn = 8.98) or the bis-hydrated complex [Mn(pmpa)] (pMn = 8.1 calculated from data obtained in 0.1 M KCl).[13] Concerning the pMn values reported for Mn(II) complexes containing at least a coordinated water molecule, they take values generally lower than 8.3,[28,30] which highlights the difficulties in designing very stable Mn(II) complexes for application as MRI contrast agents.

^{1}H NMRD and ^{17}O NMR studies

Proton relaxivity (r_{1p}) is a measure of the efficiency *in vitro* of a paramagnetic probe to enhance the relaxation rate of water proton nuclei normalized to a 1 mM concentration of the agent. The relaxivity of $[Mn(paada)]^-$ recorded at pH 7.4 (25 °C, 20 MHz) is 4.0 mM^{-1} s^{-1}, a value that is somewhat higher than those reported for monohydrated Mn(II) complexes such as $[Mn(edta)]^{2-}$ (3.3 mM^{-1} s^{-1}) and $[Mn(dpaa)]^-$ (3.6 mM^{-1} s^{-1}, Table 2). The relaxivity determined for $[Mn(nta)]^-$ (4.3 mM^{-1} s^{-1}) is slightly higher than that of $[Mn(paada)]^-$. These results represent a clear indication that both $[Mn(nta)]^-$ and $[Mn(paada)]^-$ contain two water molecules in the inner coordination sphere.

Table 2. Parameters obtained from the simultaneous analysis of ^{17}O NMR and ^{1}H NMRD data.

	$[Mn(paada)]^-$	$[Mn(nta)]^-$	$[Mn(dpaa)]^-$ [b]	[Mn(dpaMea)][c]	$[Mn(edta)]^{2-}$ [d]
r_{1p} [b] at 25/37 °C/mM^{-1} s^{-1}	4.0/3.3	4.3/3.5	3.5/2.7	5.3/4.2	3.3/2.8
$k_{ex}^{298}/10^7$ s^{-1}	90 ± 3	280 ± 10	12.6 ± 0.5	30.6	47.1
$\Delta H^{\ddagger}$/kJ mol^{-1}	28.3 ± 1.0	20.2 ± 0.9	42.7 ± 1.0	28.1	33.5
τ_R^{298}/ps	40.1 ± 0.5	37.2 ± 0.8	47.6 ± 0.2	47.8	57
E_r/kJ mol^{-1}	22.6 ± 0.5	18.9 ± 0.5	22.8 ± 0.4	25.3	21.8
τ_V^{298}/ps	12.0 ± 2.0	16.0 ± 4.0	19.4 ± 0.2	39.2	27.9
E_v/kJ mol^{-1}	1.0[a]	1.0[a]	1.0[a]	1.0[a]	1.0[a]
$D_{MnH}^{298}/10^{-10}$ m^2 s^{-1}	23[a]	23[a]	22.4[a]	22.4[a]	23.1
E_{DMnH}/kJ mol^{-1}	20[a]	20[a]	17.3[a]	17.3[a]	18.9
$\Delta^2/10^{19}$ rad^2 s^{-2}	12.8 ± 3.7	4.1 ± 1.2	5.5 ± 0.2	2.38	6.9
$A_O/\hbar/10^6$ rad s^{-1}	−38.6 ± 0.3	−47.5 ± 0.3	−31.5 ± 0.6	−45.8	−40.5
r_{MnH}/Å	2.830[a]	2.777[a]	2.756[a]	2.74[a]	2.83[a]
a_{MnH}/Å	3.6[a]	3.6[a]	3.6[a]	3.6[a]	3.6[a]
q^{298}	2[a]	2[a]	1[a]	2[a]	1[a]

[a] Parameters fixed during the fitting procedure. [b] Data from ref. 9. [c] Data from ref. 1b. [d] Data from ref. 33.

The relaxivity of $[Mn(paada)]^-$ remains constant in a broad pH range (*ca.* 5–11), and increases below pH 5 as a consequence of the dissociation of the complex (Fig. 2). This is confirmed by the speciation diagram obtained with the equilibrium constants reported in Table 1, which shows that the dissociation of the complex occurs at pH < ∼5 (Fig. 2).

^{1}H NMRD (proton Nuclear Magnetic Relaxation Dispersion) profiles of aqueous solutions of $[Mn(nta)]^-$ and $[Mn(paada)]^-$ (Fig. 3) were recorded in the range of proton Larmor frequencies of 0.01–70 MHz, which corresponds to magnetic field strengths from 2.343×10^{-4} to 1.645 T. The relaxivities of the two complexes are rather similar in the range 20–60 MHz, but differ considerably at low fields (<1 MHz). At low magnetic fields, relaxivity is dominated by the relaxation of the electron spin, which is modulated by fluctuations of the zero field splitting (ZFS) energy.

The ^{17}O NMR reduced transverse relaxation rates ($1/T_{2r}$) and chemical shifts ($\Delta\omega_r$) of $[Mn(nta)]^-$ and $[Mn(paada)]^-$ were measured as a function of temperature to gain information on the exchange rate of the coordinated water molecules and the hydration number of the complexes. The $1/T_{2r}$ values increase with decreasing temperature over the full temperature range from approximately 0 to 80 °C, which is typical of systems under the fast exchange regime (Fig. 4). Under these conditions the transverse relaxation rates do

not provide direct information on the hydration state of the complexes.[31] Thus, we performed a simultaneous fit of the ^{1}H NMRD and ^{17}O NMR data to confirm the presence of two coordinated water molecules, and to obtain information on the physicochemical parameters that determine the relaxivity of these complexes. The results of the fits are shown in Fig. 3 and 4, while the fitted parameters are listed in Table 2 and compared with the parameters reported previously for related Mn(II) complexes.

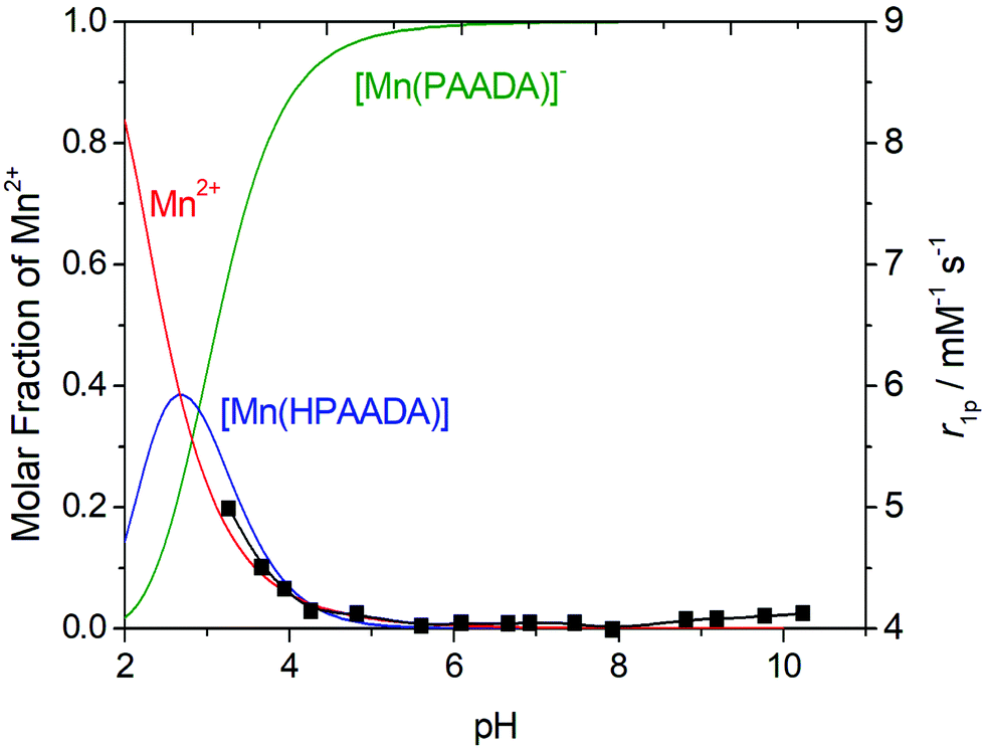

Fig. 2. Proton relaxivity (r_{1p}) of [Mn(paada)]$^{-}$ as a function of pH (squares) and species distributions calculated with the stability constants reported in Table 1 (25 °C, 0.15 M NaCl).

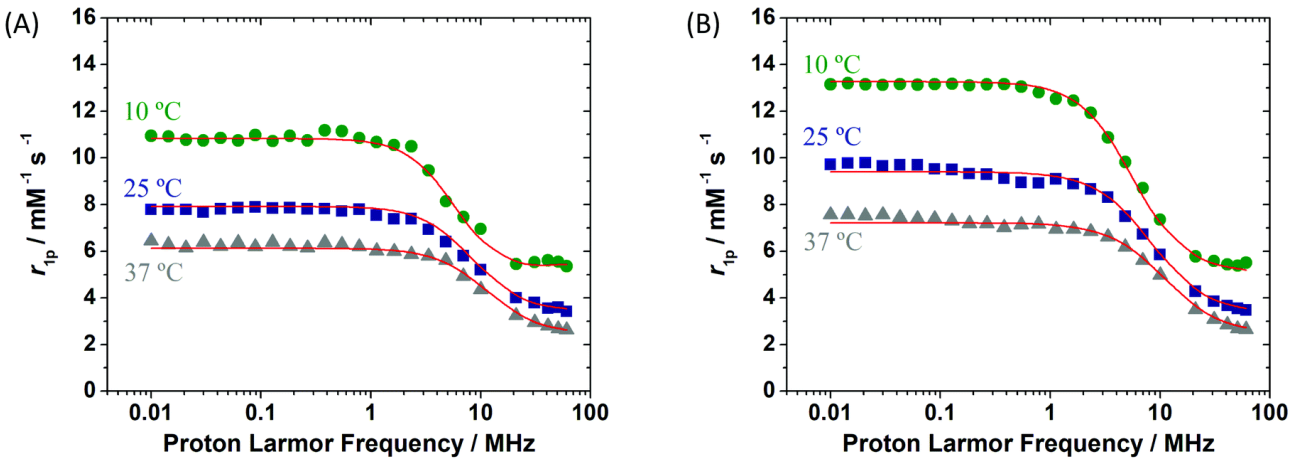

Fig. 3. ^{1}H NMRD profiles recorded at different temperatures for [Mn(paada)]$^{-}$ (A) and [Mn(nta)]$^{-}$ (B). The lines represent the fit of the data as explained in the text.

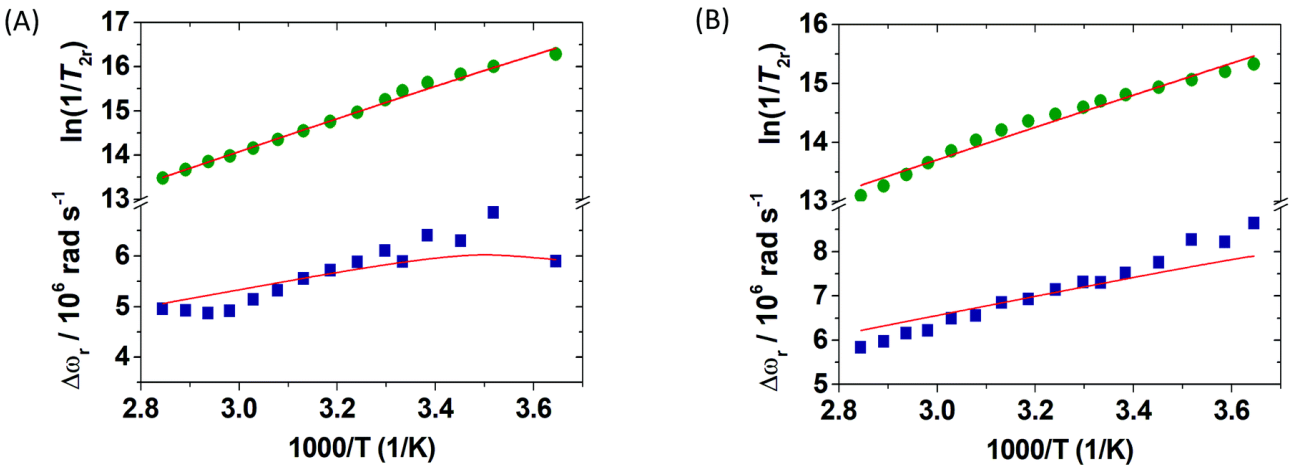

Fig. 4. Reduced transverse ^{17}O NMR relaxation rates and chemical shifts *versus* reciprocal temperatura measured for $[Mn(paada)]^-$ (A) and $[Mn(nta)]^-$ (B) at 11.74 T. The lines represent the fit of the data as explained in the text.

A rather large number of structural and dynamic molecular parameters describe the NMRD and ^{17}O NMR relaxation data and ^{17}O NMR chemical shifts. As a result, a reliable analysis requires fixing some of these parameters during the least-squares fit of the data. Thus, we fixed the distance of closest approach for the outer-sphere contribution a_{MnH} at 3.6 Å, while the distances between the Mn(II) ion and the proton nuclei of the coordinated water molecules (r_{MnH}) were fixed at the average values obtained from DFT calculations (2.830 and 2.777 Å for $[Mn(paada)]^-$ and $[Mn(nta)]^-$, respectively). The diffusion coefficient, D^{298}_{MnH}, and its activation energy, E_{DMnH}, were fixed to common values, while the number of water molecules in the inner coordination sphere of Mn(II) was fixed to $q = 2$ (Table 2).

The water exchange rate determined for $[Mn(paada)]^-$ ($k^{298}_{ex} = 90 \times 10^7$ s^{-1}) is considerably higher than that of $[Mn(dpaa)]^-$ ($k^{298}_{ex} = 12.6 \times 10^7$ s^{-1}), while the water exchange of $[Mn(nta)]^-$ is about three times faster than that of $[Mn(paada)]^-$. The water exchange obtained for $[Mn(nta)]^-$ ($k^{298}_{ex} = 280 \times 10^7$ s^{-1}) is higher than that reported by Hunt using only ^{17}O NMR data obtained at low magnetic field ($k^{298}_{ex} = 150 \times 10^7$ s^{-1}).[32] The values obtained for the rotational correlation time (τ^{298}_R) are typical of small Mn(II) complexes (*i.e.* $[Mn(edta)]^-$).[33]

The ^{17}O hyperfine coupling constants ($A_O/\hbar$) fall within the range typically observed for small Mn(II) complexes (-25×10^6 to -47×10^6 rad s^{-1}).[34] Finally, the parameters related to the electron spin relaxation of the metal ion (the electronic correlation time for the modulation of the zero-field-splitting interaction, τ_V, and the mean square zero-field-splitting energy, Δ^2) are also similar to those obtained for other Mn(II) complexes (Table 2). The fits provide a larger Δ^2 value for $[Mn(paada)]^-$ compared to $[Mn(nta)]^-$, which might be related to the different coordination environment of the metal ion in the two complexes (see below).

Theoretical calculations

DFT calculations (TPSSh/def2-TZVP, see computational details below) were carried out to gain insight into the structures of the $[Mn(paada)]^-$ and $[Mn(nta)]^-$ complexes. In these calculations, we included two inner-sphere water molecules and up to four second-sphere water molecules. Additionally, bulk solvent effects were included by using a polarized continuum model (PCM). This mixed cluster-continuum approach was shown to provide accurate Mn–O_{water} distances and ^{17}O and ^{1}H hyperfine coupling constants.[35] The optimized structure of the $[Mn(nta)(H_2O)_2]^-\cdot 4H_2O$ system shows a distorted octahedral coordination around the metal ion (Fig. 5). The coordinated water molecule in *trans* with respect to the amine nitrogen atom of the ligand presents a significantly shorter Mn–O_{water} distance (Mn–O(2w) = 2.201 Å) than the water molecule

in *cis* position (Mn–O(1w) = 2.264 Å). The metal coordination environment in $[Mn(paada)(H_2O)_2]^-\cdot 4H_2O$ can be described as pentagonal bipyramidal, in which the equatorial plane is defined by the donor atoms of the picolinate unit, the amine nitrogen atom, an oxygen atom of a carboxylate group (O2) and an inner-sphere water molecule. An oxygen atom of a carboxylate group of the ligand (O1) and the second coordinated water molecule (O2w) define the apical positions. The bond distances involving apical donor atoms are shorter than those of donor atoms lying in the equatorial plane, as usually observed for pentagonal bipyramidal Mn(II) complexes.[36] Thus, the faster water exchange determined for $[Mn(paada)(H_2O)_2]^-$ compared to $[Mn(dpaa)(H_2O)_2]^-$ is likely related to the presence of a labile water molecule occupying a coordination position at the equatorial plane of the pentagonal bipyramidal coordination polyhedron in the former. In the case of $[Mn(nta)(H_2O)_2]^-$, the water exchange process likely follows an associatively activated mechanism, given the preference of Mn(II) for coordination numbers 6 and 7.

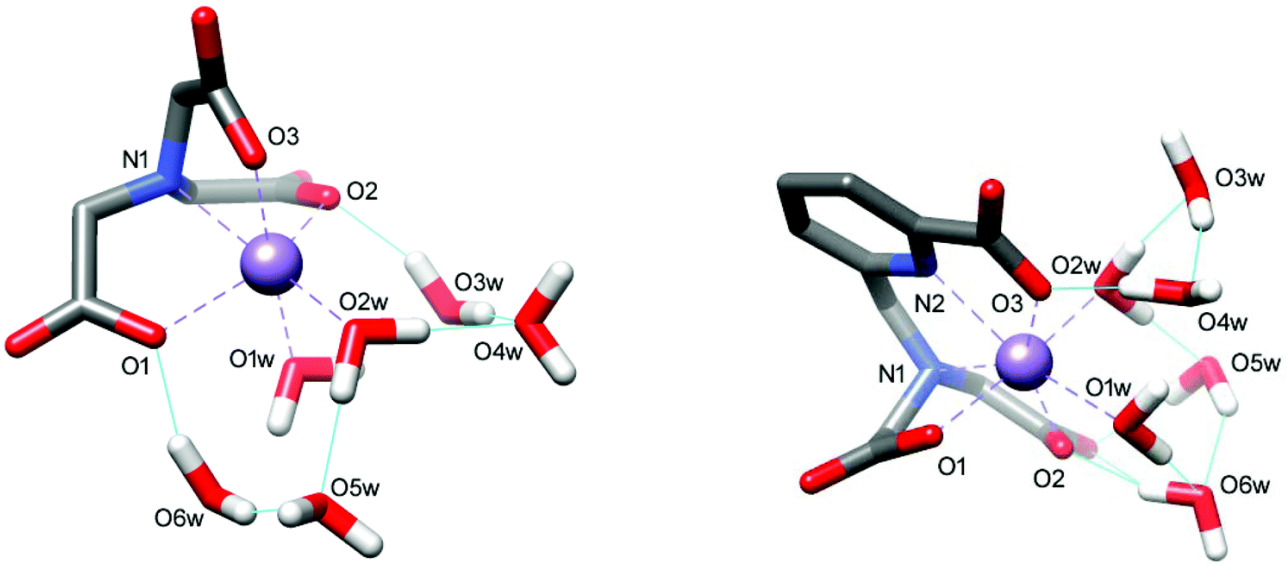

Fig. 5. Structures of the $[Mn(nta)(H_2O)_2]^-\cdot 4H_2O$ (left) and $[Mn(paada)(H_2O)_2]^-\cdot 4H_2O$ (right) systems obtained with DFT calculations (TPSSh/Def2–TZVP). Calculated bond distances (Å): $[Mn(nta)(H_2O)_2]^-\cdot 2H_2O$, Mn–N(1), 2.339; Mn–O(1), 2.171; Mn–O(2), 2.201; Mn–O(3), 2.146; Mn–O(1w), 2.264; Mn–O(2w), 2.202. $[Mn(paada)(H_2O)_2]^-\cdot 4H_2O$, Mn–N(1), 2.500; Mn–N(2), 2.361; Mn–O(1), 2.132; Mn–O(2), 2.287; Mn–O(3), 2.262 Mn–O(1w), 2.274; Mn–O(2w), 2.217.

The ^{17}O hyperfine coupling constants ($A_O/\hbar$) of the coordinated water molecules were calculated using the methodology described earlier.[35] These calculations yielded average values of $A_O/\hbar = -43.9 \times 10^6$ and -49.1×10^6 rad s^{-1} for $[Mn(nta)(H_2O)_2]^-\cdot 4H_2O$ and $[Mn(paada)(H_2O)_2]^-\cdot 4H_2O$, respectively. These values are in good agreement with the experimental data obtained from the analysis of the ^{17}O NMR chemical shifts and relaxation data, which confirms that the hydration number of $q = 2$ assumed for the fit of NMRD and ^{17}O NMR data is correct.

The values of the mean square zero field splitting (ZFS) energy obtained from the analysis of the ^{17}O and NMRD data of $[Mn(paada)(H_2O)_2]^-$ and $[Mn(nta)(H_2O)_2]^-$ are rather different ($\Delta^2 = 12.8$ and 4.1×10^{19} rad^2 s^{-2}, respectively, Table 2). Different studies have pointed out that the relaxation of the electron spin in both Mn(II) and Gd^{3+} complexes is the result of both the static and transient mechanisms.[37,38] The transient mechanism is expected to dominate for systems with high symmetry, in which the static ZFS is very small. For complexes with lower symmetry of the coordination environment, such as those investigated here, both the static and transient mechanisms likely contribute to the Δ^2 values obtained from relaxation data. The

calculation of ZFS parameters of Mn(II) and Gd^{3+} complexes using DFT was found to be problematic, with the results depending critically on the functional employed.[38,39] Thus, we carried out *ab initio* calculations based on the complete active space self-consistent field model, with an active space defined by the five electrons occupying the Mn-based 3d orbitals (CAS(5,5)). The effects of dynamic correlation were subsequently included by using *N*-electron valence perturbation theory to second order (NEVPT2). These CASSCF/NEVPT2 calculations provided very similar ZFS parameters with $D = -0.0497$ cm^{-1} and $E/D = 0.2045$ for $[Mn(nta)(H_2O)_2]^- \cdot 4H_2O$ and $D = -0.0526$ cm^{-1} and $E/D = 0.0908$ for $[Mn(paada)(H_2O)_2]^-$, which result in $\Delta = 0.043$ cm^{-1} and $\Delta^2 = 6.6 \times 10^{19}$ $rad^2\ s^{-2}$ for the two systems. The agreement between the experimental and calculated values of Δ^2 is very good for $[Mn(nta)(H_2O)_2]^-$, given the difficulties of calculating accurate ZFS parameters with *ab initio* methods. For $[Mn(paada)(H_2O)_2]^-$ the experimental ZFS is larger than that estimated with CASSCF/NEVPT2 calculations, which might be related to a more important contribution of the transient mechanism, which arises from fluctuations of the ZFS energy rather than its average value.

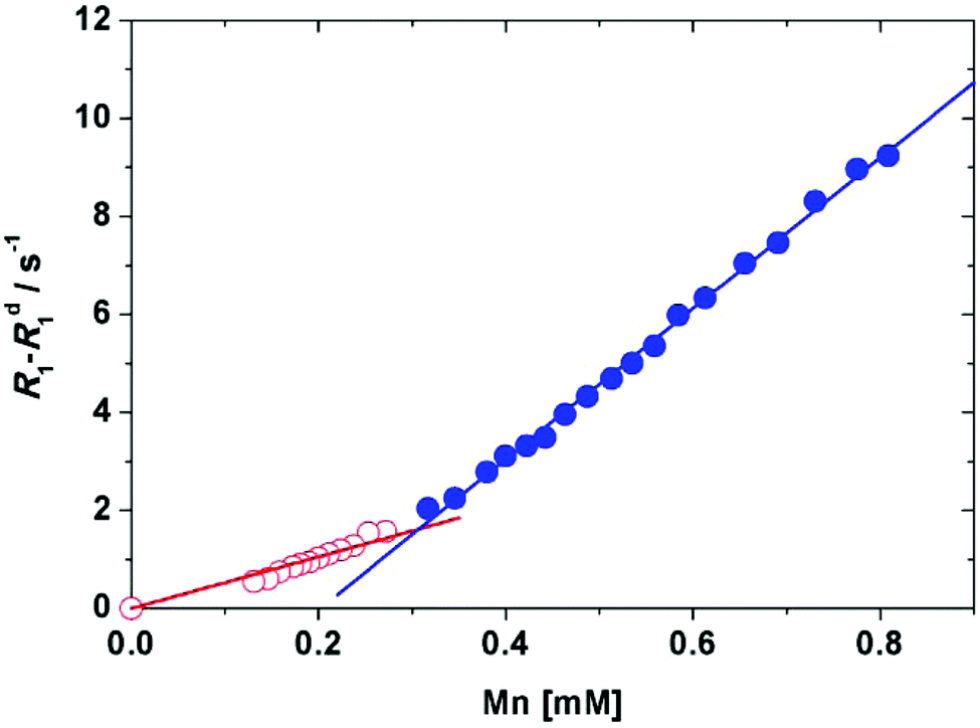

Fig. 6. Plot of the water ^1H longitudinal relaxation rate at 20 MHz and 298 K as a function of the total Mn(II) concentration for $[Mn(C_{12}Opaada)]^-$ and least-squares fit according to eqn (4) and (5).

Characterisation of the lipophilic derivative $[Mn(C_{12}Opaada)]^-$

Typically, the relaxivity of a discrete paramagnetic ion chelate in aqueous media is assessed through the measurement of the water proton relaxation rate, $R_1 = (1/T_1)$ as a function of the concentration of the metal ion over a range of about 0–3 mM. The data follows a linear behaviour and the relaxivity of the chelate, r_{1p}, corresponds to the slope of the line. However, in the case of lipophilic complexes able to self-aggregate into supramolecular assemblies, large deviations from this simple behaviour are observed. In the case of $[Mn(C_{12}Opaada)]^-$ the experimental data, measured at 20 MHz and 298 K, are reported in Fig. 6. In the concentration range 0.8 to 0.3 mM, a linear relationship is observed that corresponds to a high relaxivity

value (15.4 ± 0.2 mM^{-1} s^{-1}). By lowering the concentration, a second linear region is then observed (concentration range 300 to 100 μM) characterised by a pronounced change in the slope (5.3 ± 0.1 mM^{-1} s^{-1}). The value of the slope of this line corresponds to relaxivity values typical of rapidly rotating, low molecular weight Mn(II) complexes (Table 2).[33] This behaviour is very similar to that observed by Forgács and co-workers for Mn(dpac12a), a Mn(II) complex functionalised with a $–C_{12}$ hydrocarbon chain.[9] Similarly, we can attribute the variation of relaxivity to the formation of micelles, which are characterised by a slowed rotational mobility and therefore by an increase in r_{1p}. The point of intersection between the two straight lines defines the critical micelle concentration (*cmc*) that for $[Mn(C_{12}Opaada)]^-$ assumes the value of 0.31 ± 0.01 mM, slightly higher than for Mn(dpac12a) (0.096 mM).[9]

In the region above the *cmc*, the relaxation rate is given by the contribution of the monomeric complex (at the concentration corresponding to the *cmc*) and of the micellar aggregate. Therefore, the paramagnetic contribution to the observed relaxation rate assumes the form reported in eqn (4), where $r^{n.a.}{}_1$ and $r^a{}_1$ correspond to the relaxivity values of the non-aggregated and aggregated forms, respectively, $R^d{}_1$ is the relaxation rate of pure water (0.38 s^{-1} at 20 MHz and 298 K) and *C* is the analytical concentration of the Mn(II) complex:

$$R_1^{\mathrm{obs}} - R_1^{\mathrm{d}} = (r_1^{\mathrm{n.a.}} - r_1^{\mathrm{a}}) \times cmc \; + r_1^{\mathrm{a}} \times C. \qquad (4)$$

On the other hand, the relaxivity of the discrete complexes, $r^{n.a.}{}_1$, is expressed by the following equation:

$$R_1^{\mathrm{obs}} - R_1^{\mathrm{d}} = r_1^{\mathrm{n.a.}} \times C. \qquad (5)$$

By fitting the data to eqn (4) and (5) the parameters *cmc*, $r^{n.a.}{}_1$ and $r^a{}_1$ can be obtained (Table 3).

The method based on the fluorescence emission of pyrene (Py) was also used to determine the *cmc* at ionic strength of 0.15 M (NaCl) and in the absence of NaCl.[40] The monomer fluorescence spectrum of Py shows significant fine vibrational structure. The vibration bands show strong dependence on solvent environment. The ratio of the fluorescence emission intensities due to third and first vibration peaks increases as the polarity of the solvent decreases. In the absence of micelles (bellow *cmc*), Py senses the water environment, where $I_3/I_1 \sim 0.65$; above the *cmc* when micelles are formed, Py molecules are hosted in the interior of the micelles due to the high hydrophobicity of Py, and consequently the I_3/I_1 ratio shows a sharp increase within a narrow range of the surfactant concentration. Taken the *cmc* as the lower surfactant concentration above which micelles form (Fig. 7), these measurements provide a *cmc* for $[Mn(C_{12}Opaada)]^-$ of 0.32 mM at pH 7.4 and 0.15 M of NaCl, and of 0.56 mM at pH 7.4 in the absence of added salt. The *cmc* obtained at 0.15 M NaCl ionic strength is in excellent agreement with that determined by the relaxometric method (0.31 ± 0.01 mM). Increasing the ionic strength of the solution lowers the *cmc*, as would be expected.

Table 3. Best fit parameters obtained from the analysis of the NMRD profiles of $[Mn(C_{12}Opaada)]^-$ below and above the cmc (25 °C)

	Below *cmc*	Above *cmc*
r_{1p} [b] at 25 °C/mM^{-1} s^{-1}	5.3	15.4
k_{ex}^{298}k/10^7 s^{-1}	90[a]	90[a]
τ_{RG}^{298}/ps	71 ± 4	1920 ± 110
τ_{RL}^{298}/ps	—	90 ± 5
S^2	—	0.22 ± 0.01
τ_V^{298}/ps	14 ± 1	12.0 ± 2.0
D_{MnH}^{298}/10^{-10} m^2 s^{-1}	23[a]	23[a]
Δ^2/10^{19} rad^2 s^{-2}	15.0 ± 1.4	3.1 ± 0.6
r_{MnH}/Å	2.830[a]	2.83[a]
a_{MnH}/Å	3.6[a]	3.6[a]
q^{298}	2[a]	2[a]

[a] Parameters fixed during the fitting procedure. [b] 20 MHz.

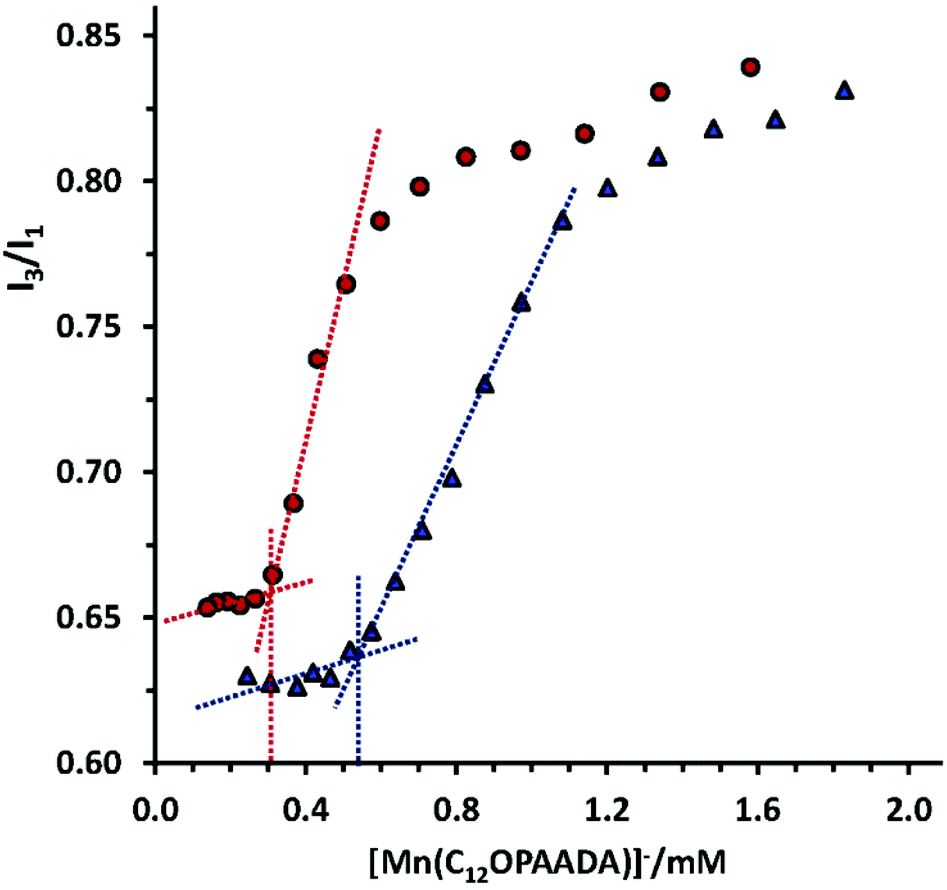

Fig. 7. Ratio of the fluorescence emission intensities corresponding to third (I_3) and first (I_1) vibrational bands of pyrene (2.04 μM) as a function of the surfactant concentration $[Mn(C_{12}Opaada)]^-$ at: (●) pH 7.46 and [NaCl] = 0.15 M; (▲) pH 7.43 in the absence of sodium chloride.

The ^{1}H NMRD profile below *cmc* exhibits the typical shape and amplitude of low molecular weight Mn(II) complexes (Fig. 8). It shows a plateau at low fields, followed by a dispersion around 3–4 MHz and then a region of nearly constant relaxivity at higher fields (≥20 MHz). The data analysis was carried out by fixing to two the number of inner sphere water molecules, at a distance of 2.83 Å and with a residence lifetime of 5 ns (298 K). Under these conditions, the relaxivity is largely controlled by the rotational dynamics, which is expressed in terms of the rotational correlation time (τ_R = 71 ± 4 ps). The τ_R value, *ca.* 77% longer than for [Mn(paada)(H_2O)]$^-$, is influenced by the functionalization of the chelate with the aliphatic chain, which increases the molecular size. On the other hand, the electronic relaxation parameters are quite similar to those of the parent complex, suggesting an analogous coordination geometry: τ_V = 14.2 ± 1.1 ps and Δ^2 = 15.0 ± 1.4 × 10^{19} s^{-2}.

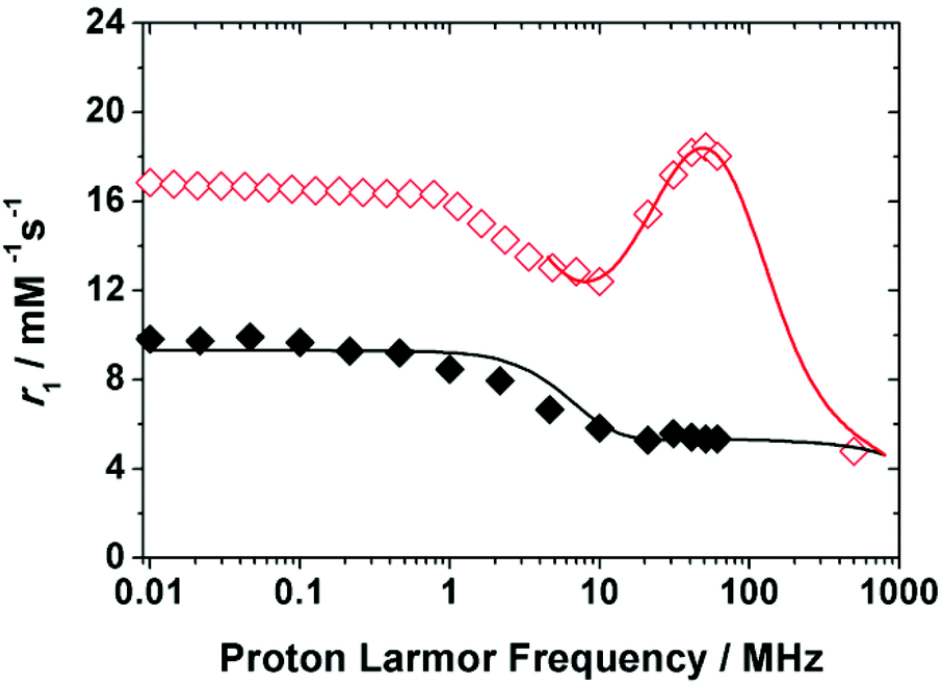

Fig. 8. $1/T_1$ ^{1}H NMRD profiles, at 298 K, of the non-aggregated (◆) aggregated (◇) form of [Mn(C_{12}Opaada)]$^-$. The solid lines are calculated with the parameters reported in Table 3.

The NMRD profile of the aggregated form of the complex exhibits a different amplitude and shape, characterised by a broad peak centred about 40 MHz, typical of slowly tumbling systems (Fig. 8).[41] The portion of the profile at high fields (>3 MHz) was fitted considering the occurrence of a local internal rotation superimposed to the global tumbling of the micelle (Lipari-Szabo approach).[42] Given the large number of parameters, some of them were fixed at known or reasonable values according to a well-established procedure. In the best-fit procedure the hydration number *q* was set to two, as for the parent complex, the Mn–H_w distance r_{MnH} was set to 2.83 Å, the distance of closest approach of the outer sphere solvent molecules to Mn(II), *a*, was fixed to 3.6 Å, while for the water-solute relative diffusion coefficient, *D*, a value of 2.3 × 10^{-5} cm^2 s^{-1} was used (25 °C). The least-square analysis was carried out by using as adjustable parameters the electron spin relaxation parameters (τ_v and Δ^2), the correlation times describing global (τ_{RG}) and local (τ_{RL}) motions and the order parameter S^2, whose value is comprised between 0 (isotropic internal motion) and 1 (completely restricted motion). The results of the fit yield τ_{RG} = 1.9 ± 0.3 ns and τ_{RL} = 90 ± 6 ps, with S^2 = 0.21 ± 0.01, indicating that relaxivity is limited by the local rotational flexibility (Table 3).

Interaction with BSA

Following a non-covalent binding interaction with a macromolecular substrate, the relaxivity of a paramagnetic chelate shows a marked enhancement (at intermediate fields) because of the pronounced variation (elongation) of τ_R passing from the rapidly rotating Mn(II) complex to the slowly tumbling supramolecular adduct. The Proton Relaxation Enhancement (PRE) technique is a non-separative methodology that enables to assess the binding parameters by measuring and analysing the changes in the NMR relaxation rates of the solvent water protons following the addition of increasing amounts of a macromolecule to a solution of the paramagnetic metal complex.[43]

We have investigated the binding interaction of $[Mn(C_{12}Opaada)]^-$ with BSA using the PRE procedure at 20 MHz and 298 K. We have utilized a 0.11 mM aqueous solution of the complex and made several additions of the protein to obtain concentrations in the range *ca.* 0.02–0.7 mM (Fig. 9).

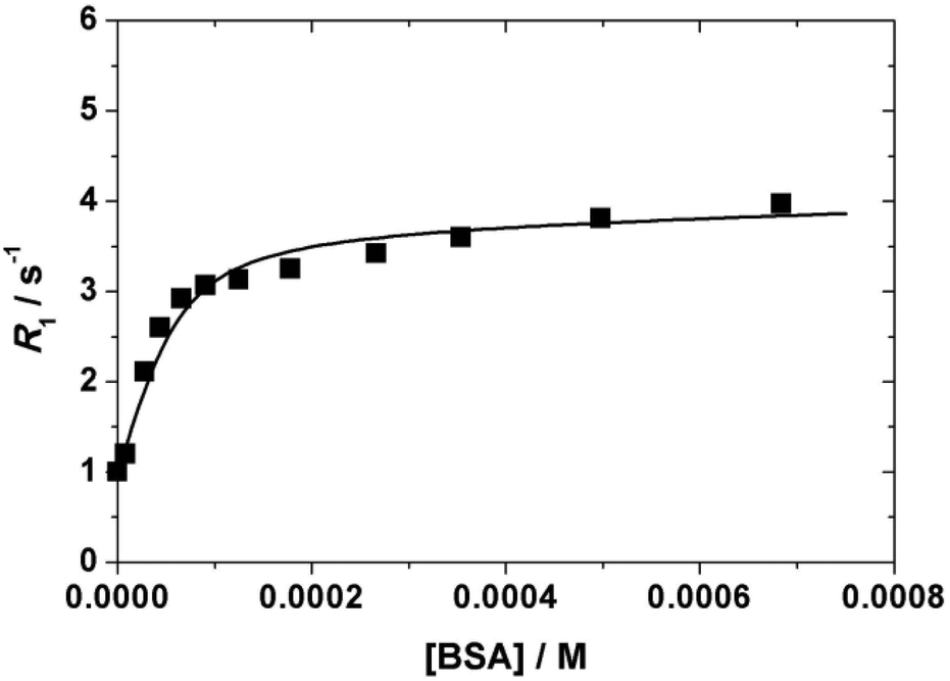

Fig. 9. Water proton relaxation rate of a 0.11 mM aqueous solutions of $[Mn(C_{12}Opaada)]^-$ as a function of increasing amounts of BSA, measured at 20 MHz and 298 K.

The observed relaxation rate, R^{obs}_1, increases with the concentration of BSA (hence with the fraction of bound complex) and tends to an asymptotic value, which depends on the relaxivity of the bound complex, r^b_1, following a binding isotherm (Fig. 9). The nonlinear fitting of the experimental data according to the PRE equations provides a fairly accurate estimation of the relaxivity of r^b_1 (30.5 ± 0.6 mM^{-1} s^{-1}) and of the $n \times K_A$ (5.6×10^4 M^{-1}) term, where n represents the number of equivalent and independent binding sites and K_A is the affinity constant. The best results are obtained with n between 1 and 2. These data are in perfect agreement with those obtained by spectrofluorimetric titration (see below). As compared to [Mn(DPAC12A)], a related complex bearing a pendant $–C_{12}$ alkyl chain, the affinity constant is slightly lower whereas the relaxivity of the adduct is twice as large ($K_A = 1.3 \times 10^5$ M^{-1} and r^b_1 = 15.5 mM^{-1} s^{-1} for [Mn(DPAC12A)]).[9] Probably, this difference simply reflects the different state of hydration of the two complexes, $q = 1$ for [Mn(DPAC12A)] and $q = 2$ for $[Mn(C_{12}Opaada)]^-$. Lower association constants with Human Serum Albumin were reported for Mn(II) macrocyclic ligands functionalized with benzyl groups.[30c]

The interactions of BSA with ligands H_3paada and H_3C_{12}Opaada, either in the absence or in the presence of Mn(II) at 1 : 1 metal : ligand (Mn : L) ratio, were also investigated by fluorimetric titration at three temperatures (15, 25 and 36 °C) in 10 mM Tris-HCl buffered solutions at pH 7.4. Under these experimental conditions, according to the pK_a values listed in Table 1, both ligands are ionic compounds in the absence of Mn(II). In fact, the concentration of $Hpaada^{2-}$ can be estimated as 4-fold that of $paada^{3-}$. A similar situation is expected for the hydrophobic ligand H_3C_{12}Opaada assuming that the presence of a hydrocarbon chain $-OC_{12}H_{25}$ has little effect on the pK_a values of the basic or acidic head groups in water. The Mn(II) complexes are negatively charged due to the high stability constant of the $[Mn(paada)]^-$ species.

On the other hand, BSA has two tryptophan residues that possess intrinsic fluorescence and usually dominate the protein fluorescence when the excitation is performed at $\lambda_{ex} \geq 290$ nm.[44] It is necessary to remark that neither the free ligands nor the Mn(II) complexes show fluorescence. Furthermore, the addition of Mn(II) (*e.g.* 52 μM) on an aqueous buffered solution of BSA (5.2 μM) has no effect on the emission spectrum of BSA. On the contrary, the fluorescence intensity of BSA decreases as the concentrations of the ligand (H_3paada or H_3C_{12}Opaada) or the corresponding Mn(II) complexes increase. However, the overall effect induced by the addition of the substrate on the intrinsic fluorescence of the protein is quite different.

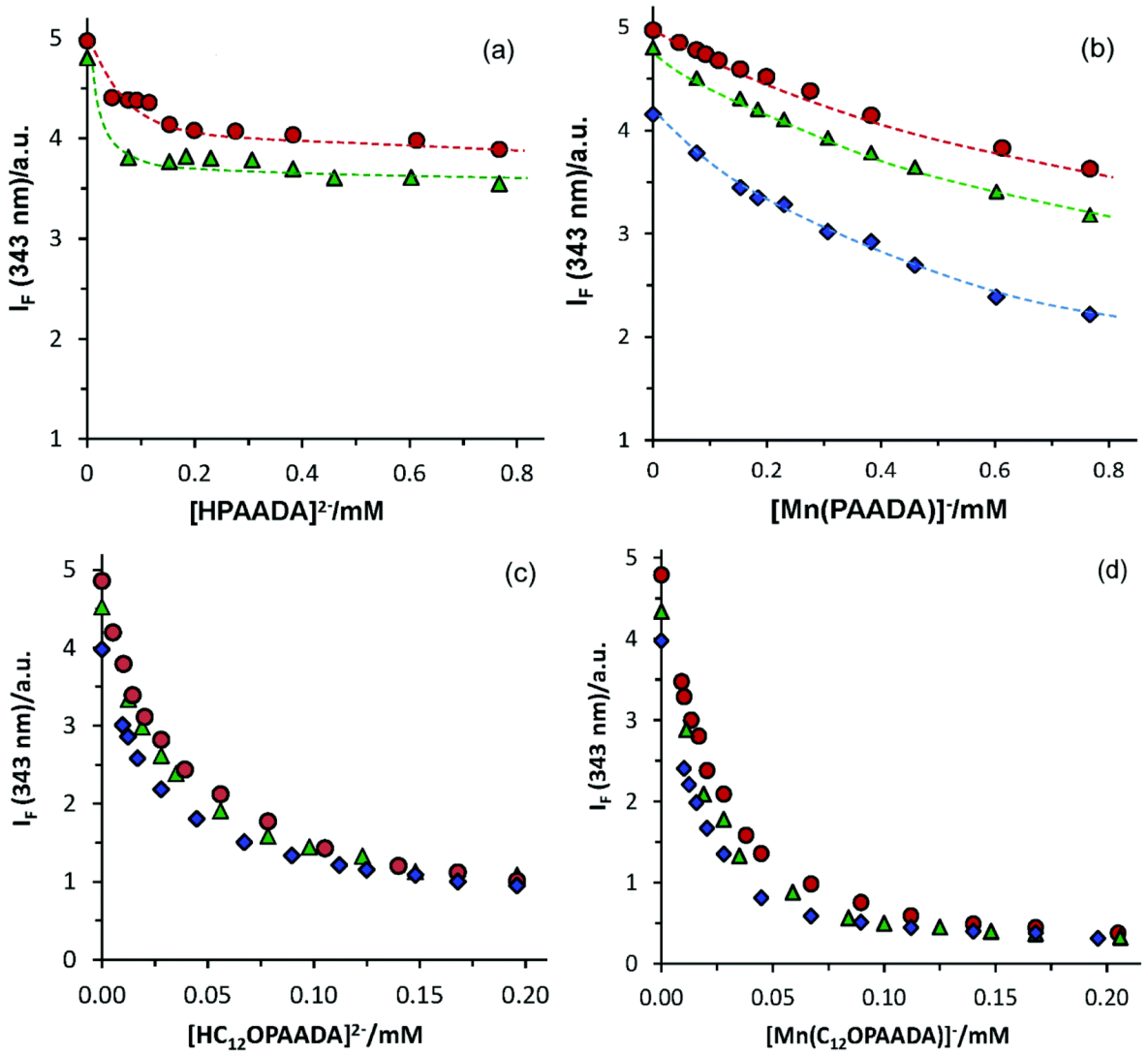

Fig. 10. The emission fluorescence intensity of BSA (5.2 μM) as a function of ligand concentration in the absence of Mn(II) (a) and (c), and in the presence of Mn(II) (b) and (d), at pH 7.4 in 10 mM Tris-HCl buffer, measured at 15 (•), 25 (▲), and 36 °C (◆).

Fig. 10 shows the decrease of the fluorescence intensity, I_F, of BSA read at the maximum wavelength emission of 343 nm as a function of ligand concentration varied in the range of 0.07 to 0.8 mM for H_3paada and from 13 to 200 μM for the case of H_3C_{12}Opaada. As a first observation, if the binding of the ligand does not introduce conformational changes in the protein, the value of the fraction θ of the sites of the protein occupied by the ligand can be determined as $\theta = (I_{Fo} - I_F)/(I_{Fo} - I_{F\infty})$, where I_{Fo} is the fluorescence in the absence of ligand (the quencher, Q); I_F is the fluorescence at a given [Q], and $I_{F\infty}$ represents the protein fluorescence "saturated" of quencher.[45]

Taking the last value as $I_{F\infty} \approx 0.3$, see Fig. 8(d), one estimates the fraction of protein sites occupied at 0.10 mM of each ligand and 15 °C as 15, 30, 85, and 100%, respectively for $Hpaada^{2-}$, $[Mn(paada)]^-$, $HC_{12}Opaada^{2-}$ or $[Mn(C_{12}Opaada)]^-$, which follows the normal trend of increasing the quencher hydrophobicity. The ligand complexed with Mn(II) shows stronger binding to the protein than the free ligand, but the presence of the hydrophobic hydrocarbon chain $–OC_{12}H_{25}$ determines the hydrophobic interaction with the protein. The fluorescence quenching by $Hpaada^{2-}$ (and/or $paada^{3-}$) does not show a gradual variation with [Q], which evidences that the ligand interactions with the protein surface are dominated mainly by electrostatic effects; in the other cases, the fluorescence decreases gradually as the ligand concentration increases.

By assuming a 1 : 1 stoichiometry for the P·Q complex (P and Q stand for the protein and quencher, respectively), the binding equilibrium constant, K_b, is represented in eqn (6). Given that the measured fluorescence intensity is only due to the protein and taking into account that the protein concentration is much lower than that of the quencher, $[P]_o \ll [Q]_o$, then $I_{Fo} = \alpha_o[P]_o$ (being $\alpha_o = 2.3I_o\phi\varepsilon\ell$ the proportionality coefficient between the fluorescence intensity and the protein concentration, *i.e.* $I_F = 2.3I_o\phi\varepsilon\ell[P]_o$ with I_o the intensity of excitation source, ϕ fluorescence quantum yield, ε molar absorptivity at the excitation wavelength, and ℓ the path length) and $I_F = \alpha_o[P] + \alpha_1[P\cdot Q]$.

$$P + Q \rightleftharpoons P \cdot Q; \quad K_b = \frac{[P\cdot Q]}{[P][Q]} \tag{6}$$

The equilibrium of eqn (6) and the mass balance on protein concentration, $[P]_o = [P] + [P\cdot Q]$, leads to eqn (7), which can be rearranged in linear forms, such as the Scatchard plot (where $[(I_{Fo}/I_F) - 1]/[Q]_o$ *versus* I_{Fo}/I_F should be linear)[46] or the Benesi–Hildebrand plot transformation in the form of $[Q]_o/(I_{Fo} - I_F)$ *versus* $[Q]_o$, where K_b is obtained from the quotient of slope/intercept of the resulting straight line.[47]

$$I_F = \frac{I_F^0 + \left(\frac{\alpha_1}{\alpha_0}\right) I_F^0 K_b [Q]_o}{1 + K_b [Q]_o} \tag{7}$$

The experimental data of $I_F - [Q]_o$ were fitted to eqn (7) using a non-linear method (Fig. S5, ESI[i]). Furthermore, good linear plots were obtained in both Scatchard or Benesi–Hildebrand plots (Fig. S6 and S7, ESI[i]). The determined values of K_b along with the corresponding thermodynamic parameters are listed in Table 4. The positive values of both entropy and enthalpy changes point to hydrophobic interactions as the main driving force in the complex P·Q formation.[48] The binding of $HC_{12}Opaada^{2-}$ and the corresponding Mn(II) complex are characterised by very similar thermodynamic parameters and association constants, which suggests that the binding of the aliphatic chain of the ligand through hydrophobic forces plays a major

role. The $[Mn(paada)]^-$ complex, which lacks the aliphatic moiety, provides a much weaker binding. The binding constant obtained at 25 °C for $[Mn(C_{12}Opaada)]$ (5.51×10^4 M^{-1}) is in excellent agreement with the one obtained with the PRE method (5.6×10^4 M^{-1}), which provides confidence on the reliability of the two methods.

Table 4. Binding constants, K_b, and thermodynamic parameters of ligand-BSA complex formation obtained from the analysis of protein fluorescence quenching by the substrate.

T/K	K_b/M^{-1}	ΔS/J mol^{-1} K^{-1}	ΔH/kJ mol^{-1}	K_b/M^{-1}	ΔS/J mol^{-1} K^{-1}	ΔH/kJ mol^{-1}	K_b/M^{-1}	ΔS/J mol^{-1} K^{-1}	ΔH/kJ mol^{-1}
	$[Mn(paada)]^-$			$HC_{12}Opaada^{2-}$			$[Mn(C_{12}Opaada)]^-$		
288	705	174	34.5	3.05×10^4	120	9.7	4.55×10^4	130	11.3
298	1081			3.46×10^4			5.51×10^4		
309	1877			4.01×10^4			6.30×10^4		

Conclusions

In this work, we have reported and discussed the synthesis of the pentadentate picolinate ligand $paada^{3-}$ and the lipophilic derivative $C_{12}Opaada^{3-}$, together with a detailed characterisation of their Mn(II) complexes. The thermodynamic stability of the $[Mn(paada)]^-$ complex was found to be intermediate between those of the Mn(II) complexes formed with the hexadentate $dpaa^{3-}$ and the tetradentate nta^{3-} ligands. A detailed ^1H and ^{17}O relaxometric characterisation of the $[Mn(paada)]^-$ complex indicated the presence of two inner-sphere water molecules involved in a rather fast exchange with bulk water. The corresponding lipophilic derivative $[Mn(C_{12}Opaada)]^-$ self-assembles into micelles in aqueous solution characterised by a *cmc* of 0.31 ± 0.01 mM, as estimated by the relaxometric method. Fluorescence measurements using pyrene as a fluorescent indicator confirmed the accuracy of the *cmc* obtained by proton relaxometry and revealed a noticeable impact of the ionic strength on the measured *cmc* values.

The $[Mn(C_{12}Opaada)]^-$ complex binds with a moderate affinity to BSA, with hydrophobic interactions being the main driving force for the adduct formation. The interaction of the aliphatic chain of the ligand with the protein through hydrophobic forces plays a major role in the binding process. The formation of micelles or binding to BSA provides a straightforward strategy to improve the relaxivity of Mn(II)–based MRI contrast agents.

Experimental section

Materials and methods

All reagents and solvents were commercial and used without further purification. SiO_2 (Sigma-Aldrich, pore size 60 Å, 70–230 mesh) was used for preparative column chromatography. ^1H and ^{13}C NMR spectra were recorded at 25 °C on Bruker Avance 300 MHz and Bruker Avance III HD 400 MHz spectrometers. ESI-TOF mass spectra were recorded using a LC-Q-q-TOF Applied Biosystems QSTAR Elite spectrometer in the positive mode. Elemental analyses were carried out on a ThermoQuest Flash EA 1112 elemental analyser. FT–IR spectra were recorded using a Thermo Scientific–Nicolet is10 spectrophotometer equipped with an attenuated total reflectance (ATR) accessory.

Methyl 6-(chloromethyl)-4-(dodecyloxy)picolinate (3)

Diethyl 4-(dodecyloxy)pyridine-2,6-dicarboxylate (1.20 g, 2.94 mmol) was dissolved in methanol (40 mL) and the mixture was cooled to 0 °C. $NaBH_4$ (0.557 g, 14.70 mmol) was added in small portions over a period of 4 h. A saturated $NaHCO_3$ solution (50 mL) was added and the mixture was extracted with CH_2Cl_2 (3 × 50 mL). The combined organic layers were dried over anhydrous Na_2SO_4 and the solvent was removed under reduced pressure to yield an oily residue. The crude product was purified by column chromatography on SiO_2 using AcOEt : hexane (40 : 60) as eluent providing 1.04 g of the white solid compound (**2**). MS (ESI) *m*/*z*: 366.26 (20%) $[C_{21}H_{35}NO_4 + H]^+$; 388.25 (100%) $[C_{21}H_{35}NO_4 + Na]^+$. This intermediate was dissolved in thionyl chloride (5 mL) and the mixture was stirred at 0 °C for 4 h. The mixture was allowed to warm to room temperature and the thionyl chloride was removed in the rotary evaporator. A saturated $NaHCO_3$ solution (50 mL) was added and the mixture was extracted with CH_2Cl_2 (3 × 50 mL). The combined organic layers were dried over anhydrous Na_2SO_4 and the solvent was removed under reduced pressure to give a yellow solid. The crude product was purified by column chromatography on SiO_2 (CH_2Cl_2 to CH_2Cl_2 : MeOH 95 : 5) giving 0.221 g of a white solid. Yield 25%. The ethyl ester group of the precursor was converted into methyl ester under the conditions used for chromatographic separation. ^{1}H NMR ($CDCl_3$, 400 MHz, 25 °C, TMS): δ 7.53 (d, 1H, py, ^4J = 2.4 Hz), 7.14 (d, 1H, py, ^4J = 2.4 Hz), 4.64 (s, 2H, py–CH_2), 4.02 (t, 2H, O–CH_2, ^3J = 6.5 Hz), 3.93 (s, 3H, COO–CH_3), 1.75 (m, 2H, CH_2), 1.39 (m, 2H, CH_2), 1.20 (m, 18H, CH_2), 0.81 (t, 3H, CH_3, ^2J = 6.7 Hz). ^{13}C NMR ($CDCl_3$, 100.6 MHz, 25 °C, TMS): δ 167.01 (**C**OOCH$_3$), 165.51 (**C**$_{py}$–O), 158.65 (**C**$_{py}$–CH_2Cl), 149.05 (**C**$_{py}$–COOCH$_3$), 112.28 (**C**$_{py}$), 111.26 (**C**$_{py}$), 68.75 (**C**H$_2$–O), 53.10 (COO**C**H$_3$), 46.39 (**C**H$_2$Cl), 31.91 (**C**H$_2$), 29.64 (**C**H$_2$), 29.62 (**C**H$_2$), 29.56 (**C**H$_2$), 29.51 (**C**H$_2$), 29.34 (**C**H$_2$), 29.27 (**C**H$_2$), 28.79 (**C**H$_2$), 25.86 (**C**H$_2$), 22.68 (**C**H$_2$), 14.11 (**C**H$_3$) ppm. MS (ESI$^+$) *m*/*z*: 370.21 (23%) $[C_{20}H_{32}ClNO_3 + H]^+$; 392.20 (100%) $[C_{20}H_{32}ClNO_3 + Na]^+$. Anal. calcd for $C_{20}H_{32}ClNO_3$: C, 64.94; H, 8.72; N, 3.79. Found: C, 64.71; H, 8.64; N, 3.65%.

2,2′-(((6-Carboxy-4-(dodecyloxy)pyridin-2-yl)methyl)azanediyl) diacetic acid (H_3C_{12}Opaada)

Compound **3** (0.1915 g, 0.518 mmol) and di-*tert*-butyl 2,2′-azanediyldiacetate (0.1223 g, 0.499 mmol) were dissolved in acetonitrile (20 mL) and K_2CO_3 (0.1723 g, 1.247 mmol) were added. The mixture was stirred at room temperature for 3 days. The excess K_2CO_3 was removed by filtration and the filtrate concentrated to dryness yielding a deep yellow oil, which was purified by column chromatography on SiO_2 using AcOEt : hexane (20 : 80) as eluent giving 0.310 g of the ester intermediate **5** an oily product. The oil was dissolved in 6 M HCl (20 mL) and the mixture was stirred at room temperature 24 h. The white precipitate was isolated by filtration and washed with acetone. Addition of acetone to the filtrate provoked the precipitation of a second batch of the product. The combined white solids were dried providing a white solid (0.095 g, 0.160 mmol). Yield: 42%. ^{1}H NMR ($CDCl_3$, 300 MHz, 25 °C, TMS): δ 7.48 (s, 2H, Py), 4.04 (m, 4H, O–CH_2), 3.92 (s, 2H, Py–CH_2), 3.43 (s, 4H, CH_2–COOH), 1.75 (m, 2H, CH_2), 1.22 (s, 18H, CH_2), 0.83 (t, 3H, CH_3, ^2J = 7.1 Hz). ^{13}C NMR ($CDCl_3$, 125.8 MHz, 25 °C, TMS): δ 170.51, 166.96, 166.02, 162.44, 148.82, 111.45, 111.10, 68.46, 60.19, 52.89, 31.95, 29.70, 29.67, 29.61, 29.59, 29.38, 29.35, 28.93, 25.97, 22.72, 14.15 (**C**H$_3$) ppm. MS (ESI$^+$) *m*/*z*: 453.26 (100%) ($[C_{23}H_{36}N_2O_7 + H]^+$). IR (ATR): ν 1746 cm^{-1} (C═O). Anal. calcd for $C_{23}H_{36}N_2O_7 \cdot 2HCl$: C, 52.57; H, 7.29; N, 5.33. Found: C, 52.86; H, 6.56; N, 5.38%.

Di-*tert*-Butyl 2,2′-(((6-(methoxycarbonyl)pyridin-2-yl)methyl)azanediyl)diacetate (6)

A solution of methyl 6-(chloromethyl)picolinate (0.1878 g, 1.012 mmol) in CH_3CN (15 mL) was added dropwise to a mixture of di-*tert*-butyl 2,2′-azanediyldiacetate (0.2475 g, 1.008 mmol) and K_2CO_3 (0.7019 g, 5.079 mmol, 5 eq.) in CH_3CN (20 mL) at room temperature. The reaction mixture was stirred at room temperature for 72 h and at 50 °C for another 24 h. After filtration, the residue was washed with CH_2Cl_2 (3 × 50 mL). The organic layer was dried over anhydrous Na_2SO_4 and the solvent was removed under reduced pressure to yield a solid residue. Quantitative. ^{1}H NMR ($CDCl_3$, 300 MHz, 25 °C, TMS): δ 7.73–7.71 (d, 2H, PyH), 7.61–7.56 (t, 1H, PyH), 3.88 (s, 2H, CH_2), 3.70 (s, 3H, CH_3), 3.22 (s, 4H, CH_2), 1.18 (s, 18H,

$(CH_3)_3$). ^{13}C NMR ($CDCl_3$, 75 MHz, 25 °C, TMS): δ 170.03 (COO*t*Bu), 165.49 ($COOCH_3$), 160.35 (C–Py), 146.96 (C–Py), 137.30 (CH–Py), 126.02 (CH–Py), 123.39 (CH–Py), 80.69 ($C(CH_3)_3$), 59.71 (CH_2), 55.63 (CH_2), 52.44 (CH_3), 27.88 ($(CH_3)_3$). MS (ESI^+) *m*/*z*: 417.20 $[C_{20}H_{30}N_2O_6 + Na]^+$.

2,2′-(((6-Carboxypyridin-2-yl)methyl)azanediyl)diacetic acid (H_3paada)

Compound **6** (0.3980 g, 1.008 mmol) was dissolved in 6 M HCl (10 mL) and heated under reflux for 48 h. After cooling the mixture, the white precipitate formed was collected by filtration, washed with acetone and dried (0.300 g, 0.857 mmol). Yield 85%. ^{1}H NMR (D_2O, 300 MHz, 25 °C, TMS): δ 7.83–7.78 (t, 1H, PyH), 7.71–7.69 (d, 1H, PyH), 7.56–7.54 (d, 1H, PyH), 3.82 (s, 2H, CH_2), 3.14 (s, 4H, CH_2). ^{13}C NMR (D_2O, 75 MHz, 25 °C, TMS): δ 174.08 (CH_2**C**OOH), 172.88 (Py–**C**OOH), 153.49 (C–Py), 152.74 (C–Py), 138.83 (C–Py), 126.16 (C–Py), 123.38 (C–Py), 58.94 (CH_2), 57.24 (**C**H_2COOH). MS (ESI^+) *m*/*z*: 267.06 $[C_{11}H_{12}N_2O_6–H]^-$. Anal. calcd for $C_{11}H_{12}N_2O_6 \cdot 2HCl \cdot 0.5H_2O$: C, 37.73; H, 4.32; N, 8.00. Found: C, 37.61; H, 4.50; N, 7.67%.

Equilibrium measurements

The protonation constants of the ligand and the stability constant of the Mn(II) complex with $paada^{3-}$ were determined by potentiometric and spectrophotometric titrations. The necessary amount of sodium chloride was added to all solutions in order to keep the ionic strength at a constant value of 0.15 M, while the temperature was always 25 °C. The Hyperquad program[49] was used to fit potentiometric titration data. The calibration parameters were determined using solutions of known proton concentration, as described below, and were given to the program in order to obtain the equilibrium constants.

The spectrophotometric data were fitted with the pHab program,[50] a program designed to fit spectrophotometrical data of solutions of known pH (with $pH = -\log[H^+]$). Again, solutions of known proton concentration were used to calibrate the electrode and to find the pH of sample solutions. The UV-vis absorption spectra were recorded with a Uvikon-XS (Bio-Tek Instruments) double-beam spectrophotometer with cells of 1 cm path length. The spectra were recorded in the range 220–320 nm (100 wavelengths). The solutions were prepared one day before the measurements were carried out, to assure that the equilibrium was attained (batch method).

All potentiometric titrations were performed in a dual-wall cell that was kept at a constant temperature by circulating water from a thermostat. Nitrogen was bubbled on the surface of the solution to avoid CO_2 absorption while a magnetic stirrer was used to homogenise the solutions. A Crison microBu 2030 automatic burette equipped with 2.5 mL or 1.0 mL syringes was used to deliver the titrant. The electromotive force (emf) values were read using a Crison micropH 2000 pH-meter connected to a glass electrode (Radiometer pHG211) and a reference electrode (Radiometer REF201). The calibration procedure was described elsewhere.[7] Briefly, the electrode response at constant ionic strength is given by $E = E^{\circ\prime} + s \log[H^+]$, with E being the emf, E°′ the formal potential, and s the slope. A weak acid (Na_2HPO_4) was titrated with a standard HCl solution and with the known equilibrium constants the proton concentration was found at each point of the titration. A linear regression of *E vs*. $\log[H^+]$ yielded *s* and $E^{\circ\prime}$.

Several titrations were performed to obtain the acid–base and the complexation constants of the $paada^{3-}$ ligand with Mn(II). The ligand was in the hydrochloride form, so that it was initially titrated with sodium hydroxide. At the end of this titration, NaOH was added to deprotonate the ligand, and the basic solution was titrated with HCl in order to determine the acid–base equilibrium constants. At the end of the titration in acid media (pH ~ 2) Mn(II) was added (at the same concentration of the ligand) and the solution was titrated with NaOH until pH ~ 4, before reaching the equivalence point, to preclude precipitation. The concentration of the ligand was in the range 2.0–3.5 mM. The equilibrium was attained quickly in the

titrations of the complex except near the equivalence point. Thus, points very near the equivalence point were not used for the fitting (pH > 4).

^{1}H NMRD and ^{17}O NMR measurements

The proton $1/T_1$ NMRD profiles were recorded using a fast field-cycling Stelar SmartTracer relaxometer (Mede, Pv, Italy) over a continuum of magnetic field strengths from 0.00024 to 0.25 T (corresponding to 0.01–10 MHz proton Larmor frequencies). The temperature was controlled with a Stelar VTC-91 airflow heater equipped with a calibrated copper–constantan thermocouple (uncertainty of ±0.1 K). A Stelar Relaxometer equipped with a Bruker WP80 NMR electromagnet adapted to variable-field measurements (15–80 MHz proton Larmor frequency) was used to obtain additional data points in the range 15–70 MHz. The relaxometer is operated under computer control providing $1/T_1$ values with an absolute uncertainty of ±1%.

^{17}O NMR chemical shifts and transverse relaxation rates were recorded on a Bruker Avance III spectrometer (11.7 T) equipped with a 5 mm probe and standard temperature control unit. The solutions of the complexes were enriched to reach 2.0% of the ^{17}O isotope (Cambridge Isotope). The transverse relaxation rates were obtained from the signal width at half-height. The exact concentrations of the solutions used for ^{1}H NMRD and ^{17}O NMR measurements were determined by the BMS shift method at 11.7 T.[51]

Fluorescence measurements

Steady-state fluorescence measurements were performed on an Amincon-Bowman series 2 spectrofluorimeter equipped with thermostat bath. Excitation and emission slits were fixed at 4 and 2 nm, respectively. The excitation wavelength was set at 290 nm, and the fluorescence emission spectra were recorded at different temperatures (288, 298, and 310 K) in the wavelength range of 300–420 nm; the intensity of fluorescence, I_F, was read at the emission maximum wavelength of 343 nm. Fluorescence titration experiments were performed by keeping the concentration of BSA constant (5.2 μM) in 10 mM Tris-HCl buffer, pH 7.4 while varying either the ligand concentration or both the ligand and Mn(II) concentrations at the Mn : L ratio of 1 : 1. In the two sets of experiments, the ratio [ligand]/[BSA] was made to vary from 4 to 40, approximately. The reported pH values correspond to the sample mixture. Concentrated aqueous solutions of $MnCl_2$ were used to simply add small aliquots (*i.e.* 10–100 μL) to about 3.0 mL of a single sample solution of BSA (in a fluorimetric cuvette) and the ligand in Tris-HCl buffer; that is, the same solution was used to record both the fluorescence spectrum in the absence and presence of Mn(II). Sufficient time was leave between measurements in order to achieve the new equilibration. Corrections for the dilution of the absorbent or fluorescent material were made when necessary. The absorbance values read at the excitation wavelength (335 nm for pyrene or 290 nm for BSA) were always lower than 0.15 absorbance units to avoid inner filter effects.

Computational details

Full geometry optimizations of the $[Mn(paada)(H_2O)_2]^{-}\cdot 4H_2O$ and $[Mn(nta)(H_2O)_2]^{-}\cdot 4H_2O$ systems were performed employing DFT calculations at the M06–2X/Def2–TZVP[52,53] level employing the Gaussian 09 package (Revision E.01).[54] Solvent effects were introduced by using the polarizable continuum model (PCM). In particular, we used the integral equation formalism (IEFPCM) variant as implemented in Gaussian 09.[55] No symmetry constraints have been imposed during the optimizations. The stationary points found on the potential energy surfaces as a result of geometry optimizations were confirmed to represent energy minima rather than saddle points *via* frequency analysis. ^{17}O hyperfine coupling constants were calculated using the M06–2X functional in combination with the EPR–III[56] basis set for the ligand atoms and the aug-cc-pVTZ-J basis set for Mn.[57]

Complete Active Space Self-Consistent Field (CASSCF)[58] and *N*-electron valence perturbation theory to second order (NEVPT2)[59] calculations were performed using the ORCA program package (Release 4.0.1.2).[60] The def2–TZVP basis set[53] basis set was used throughout. CASSCF calculations were performed by using an active space including five electrons distributed into the five Mn 3d-based molecular orbitals (CAS(5,5)). The orbitals were optimised by averaging 1 sextet, 24 quartets and 75 doublet roots. NEVPT2 calculations were performed on the top of the CASSCF wave functions to account for dynamic correlation, while SOC effects were introduced by quasi-degenerate perturbation theory (QDPT).[61] Solvent effects were introduced with the universal solvation model based on solute electron density and on a continuum model (SMD).[62]

Conflicts of interest

There are no conflicts to declare.

Acknowledgements

Authors R. P.-P., I. B., E. I., C. P.-I. and D. E.-G. thank Ministerio de Economía y Competitividad (CTQ2016-76756-P) and Xunta de Galicia (ED431B 2017/59 and ED431D 2017/01) for generous financial support and Centro de Supercomputación of Galicia (CESGA) for providing the computer facilities. R. P.-P. thanks Ministerio de Economía y Competitividad for a PhD FPI grant (BES-2014-068399) and a fellowship for a short term stay in Alessandria (EEBB-I-18-13075). R. U.-V. thanks Xunta de Galicia for a PhD grant (ED481A-2018/314). M.B. and F.C. are grateful to Università del Piemonte Orientale for financial support (Ricerca locale 2016). This work was carried out within the framework of the COST CA15209 Action "European Network on NMR Relaxometry".

References

1. (*a*) M. Regueiro-Figueroa, G. A. Rolla, D. Esteban-Gómez, A. de Blas, T. Rodríguez-Blas, M. Botta and C. Platas-Iglesias, *Chem. – Eur. J.*, 2014, **20**, 17300; (*b*) A. Forgács, M. Regueiro-Figueroa, J. L. Barriada, D. Esteban-Gómez, A. de Blas, T. Rodríguez-Blas, M. Botta and C. Platas-Iglesias, *Inorg. Chem.*, 2015, **54**, 9576.

2. E. W. Price, J. F. Cawthray, G. A. Bailey, C. L. Ferreira, E. Boros, M. J. Adam and C. Orvig, *J. Am. Chem. Soc.*, 2012, **134**, 8670.

3. N. Chatterton, Y. Bretonnière, J. Pécaut and M. Mazzanti, *Angew. Chem., Int. Ed.*, 2005, **44**, 7595.

4. (*a*) E. Boros, J. F. Cawthray, C. L. Ferreira, B. O. Patrick, M. J. Adam and C. Orvig, *Inorg. Chem.*, 2012, **51**, 6279; (*b*) C. F. Ramogida, E. Boros, B. O. Patrick, S. K. Zeisler, J. Kumlin, M. J. Adam, P. Schaffer and C. Orvig, *Dalton Trans.*, 2016, **45**, 13082; (*c*) C. F. Ramogida, D. Schindler, C. Schneider, Y. L. K. Tan, S. Huh, C. L. Ferreira, M. J. Adam and C. Orvig, *RSC Adv.*, 2016, **6**, 103763; (*d*) C. F. Ramogida, J. Pan, C. L. Ferreira, B. O. Patrick, K. Rebullar, D. T. T. Yapp, K.-S. Lin, M. J. Adam and C. Orvig, *Inorg. Chem.*, 2015, **54**, 4953; (*e*) E. Boros, C. L. Ferreira, J. F. Cawthray, E. W. Price, B. O. Patrick, D. W. Wester, M. J. Adam and C. Orvig, *J. Am. Chem. Soc.*, 2012, **132**, 15726–15733.

5. C. F. Ramogida, J. F. Caethray, E. Boros, C. L. Ferreira, B. O. Patrick, M. J. Adam and C. Orvig, *Inorg. Chem.*, 2015, **54**, 2017.

6. R. Ferreirós-Martínez, D. Esteban-Gómez, C. Platas-Iglesias, A. de Blas and T. Rodríguez-Blas, *Dalton Trans.*, 2008, 5754.

7. L. Caneda-Martínez, L. Valencia, I. Fernández-Pérez, M. Regueiro-Figueroa, G. Angelovski, I. Brandariz, D. Esteban-Gómez and C. Platas-Iglesias, *Dalton Trans.*, 2017, **46**, 15095.

8. (*a*) D. M. Weekes, C. F. Ramogida, M. de G. Jaraquemada-Peláez, B. O. Patrick, C. Apte, T. I. Kostelnik, J. F. Cawthray, L. Murphy and C. Orvig, *Inorg. Chem.*, 2016, **55**, 12544; (*b*) T. W. Price, J. Gallo, V. Kubicek, Z. Böhmová, T. J. Prior, J. Greenman, P. Hermann and G. J. Stasiuk, *Dalton Trans.*, 2017, **46**, 16973.

9. A. Forgács, R. Pujales-Paradela, M. Regueiro-Figueroa, L. Valencia, D. Esteban-Gómez, M. Botta and C. Platas-Iglesias, *Dalton Trans.*, 2017, **46**, 1546.

10. M. Khannam, T. Weyhermüller, U. Goswami and C. Mukherjee, *Dalton Trans.*, 2017, **46**, 10426.

11. (*a*) C. Platas-Iglesias, M. Mato-Iglesias, K. Djanashvili, R. N. Muller, L. Vander Elst, J. A. Peters, A. de Blas and T. Rodríguez-Blas, *Chem. – Eur. J.*, 2004, **10**, 3579; (*b*) F. K. Kálmán, A. Végh, M. Regueiro-Figueroa, É. Tóth, C. Platas-Iglesias and G. Tircsó, *Inorg. Chem.*, 2015, **54**, 2345.

12. G. Tircsó, M. Regueiro-Figueroa, V. Nagy, Z. Garda, T. Garai, F. K. Kálmán, D. Esteban-Gómez, É. Tóth and C. Platas-Iglesias, *Chem. – Eur. J.*, 2016, **22**, 896.

13. B. Phukan, C. Mukherjee, U. Goswani, A. Sarmah, S. Mukherjee, S. K. Sahoo and S. C. Moi, *Inorg. Chem.*, 2018, **57**, 2631.

14. (*a*) B. Drahos, I. Lukes and E. Toth, *Eur. J. Inorg. Chem.*, 2012, 1975; (*b*) M. Kueny-Stotz, A. Garofalo and D. Felder-Flesch, *Eur. J. Inorg. Chem.*, 2012, 1987.

15. D. Pan, A. H. Schmieder, S. A. Wickline and G. M. Lanza, *Tetrahedron*, 2011, **67**, 8431.

16. (*a*) S. Cheng, L. Abramova, G. Saab, G. Turabelidze, P. Patel, M. Arduino, T. Hess, A. Kallen and M. Jhung, *J. Am. Med. Assoc.*, 2007, **297**, 1542; (*b*) T. H. Darrah, J. J. Prutsman-Pfeiffer, R. J. Poreda, M. E. Campbell, P. V. Hauschka and R. E. Hannigan, *Metallomics*, 2009, **1**, 479.

17. (*a*) T. Kanda, T. Fukusato, M. Matsuda, K. Toyoda, H. Oba, J. Kotoku, T. Haruyama, K. Kitajima and S. Furui, *Radiology*, 2015, **276**, 228; (*b*) E. Kanal and M. F. Tweedle, *Radiology*, 2015, **275**, 630; (*c*) D. R. Roberts, S. M. Lindhorst, C. T. Welsh, K. R. Maravilla, M. N. Herring, K. A. Braun, B. H. Thiers and W. C. Davis, *Invest. Radiol.*, 2016, **51**, 280; (*d*) M. Birka, K. S. Wentker, E. Lusmöller, B. Arheilger, C. A. Wehe, M. Sperling, R. Stadler and U. Karst, *Anal. Chem.*, 2015, **87**, 3321.

18. E. M. Gale, I. P. Atanasova, F. Blasi, I. Ay and P. Caravan, *J. Am. Chem. Soc.*, 2015, **137**, 15548.

19. I. Bertini, F. Briganti, Z. Xia and C. Luchinat, *J. Magn. Reson.*, 1993, **101**, 198.

20. (*a*) G. S. Loving, S. Mukherjee and P. Caravan, *J. Am. Chem. Soc.*, 2013, **135**, 4620; (*b*) E. M. Gale, S. Mukherjee, C. Liu, G. S. Loving and P. Caravan, *Inorg. Chem.*, 2014, **53**, 10748.

21. T. Storr, B. R. Cameron, R. A. Gossage, H. Yee, R. T. Skerlj, M. C. Darkes, S. P. Fricker, G. J. Bridger, N. A. Davies, M. T. Wilson, K. P. Maresca and J. Zubieta, *Eur. J. Inorg. Chem.*, 2005, 2685.

22. M. Schäferling, T. Ääritalo and T. Soukka, *Chem. – Eur. J.*, 2014, **20**, 5298.

23. C. S. Bonnet, L. Pellagatti, F. Buron, C. M. Shade, S. Villette, V. Kubicek, G. Guillaumet, F. Suzenet, S. Petoud and E. Toth, *Chem. Commun.*, 2010, **46**, 124.

24. G. Anderegg, *Pure Appl. Chem.*, 1982, **54**, 2693.

25. N. Chatterton, C. Gateau, M. Mazzanti, J. Pécaut, A. Borel, L. Helm and A. Merbach, *Dalton Trans.*, 2005, 1129.

26. A. Nonat, C. Gateau, P. H. Fries and M. Mazzanti, *Chem. – Eur. J.*, 2006, **12**, 7133.

27. A. N. Nonat, C. Gateau, P. H. Fries, L. Helm and M. Mazzanti, *Eur. J. Inorg. Chem.*, 2012, 2049.

28. B. Drahos, J. Kotek, P. Hermann, I. Lukes and E. Toth, *Inorg. Chem.*, 2010, **49**, 3224.

29. S. M. Rocklage, W. P. Cacheris, S. C. Quay, F. E. Hahn and K. N. Raymond, *Inorg. Chem.*, 1989, **28**, 477.

30. (*a*) B. Drahos, J. Kotek, I. Cisarova, P. Hermann, L. Helm, I. Lukes and E. Toth, *Inorg. Chem.*, 2011, **50**, 12785; (*b*) A. de Sa, C. S. Bonnet, C. F. G. C. Geraldes, E. Toth, P. M. T. Ferreira and J. P. Andre, *Dalton Trans.*, 2013, **42**, 4522; (*c*) A. Forgacs, L. Tei, Z. Baranyai, D. Esteban-Gomez, C. Platas-Iglesias and M. Botta, *Dalton Trans.*, 2017, **46**, 8494.

31. E. M. Gale, J. Zhu and P. Caravan, *J. Am. Chem. Soc.*, 2013, **135**, 18600.

32. M. S. Zetter, M. W. Grant, E. J. Wood, H. W. Dodgen and J. P. Hunt, *Inorg. Chem.*, 1972, **11**, 2701.

33. G. A. Rolla, C. Platas-Iglesias, M. Botta, L. Tei and L. Helm, *Inorg. Chem.*, 2013, **52**, 3268.

34. L. Tei, G. Gugliotta, M. Fekete, F. K. Kalman and M. Botta, *Dalton Trans.*, 2011, **40**, 2025.

35. (*a*) V. Patinec, G. A. Rolla, M. Botta, R. Tripier, D. Esteban-Gómez and C. Platas-Iglesias, *Inorg. Chem.* 2013, **52**, 11173; (*b*) D. Esteban-Gómez, C. Cassino, M. Botta and C. Platas-Iglesias, *RSC Adv.*, 2014, **4**, 7094.

36. G.-F. Liu, M. Filipovic, F. W. Heinemann and I. Ivanovic-Burmazovic, *Inorg. Chem.*, 2007, **46**, 8825.

37. P. H. Fries and E. Belorizky, *ChemPhysChem*, 2012, **13**, 2074.

38. C. Platas-Iglesias, D. Esteban-Gómez, L. Helm and M. Regueiro-Figueroa, *J. Phys. Chem. A*, 2016, **120**, 6467.

39. (*a*) S. Khan, R. Pollet, R. Vuilleumier, J. Kowalewski and M. Odelius, *J. Chem. Phys.*, 2017, **147**, 244306; (*b*) S. Khan, A. Kubica-Misztal, D. Kruk, J. Kowalewski and M. Odelius, *J. Chem. Phys.*, 2015, **142**, 034304.

40. A. Domínguez, A. Fernández, N. González, E. Iglesias and L. Montenegro, *J. Chem. Educ.*, 1997, **74**, 1227.

41. S. Aime, M. Botta, D. Esteban-Gómez and C. Platas-Iglesias, *Mol. Phys.*, 2018 DOI:10.1080/00268976.2018.1516898.

42. (*a*) G. Lipari and S. Szabo, *J. Am. Chem. Soc.*, 1982, **104**, 4556; (*b*) G. Lipari and S. Szabo, *J. Am. Chem. Soc.*, 1982, **104**, 4559.

43. L. Helm, J. R. Morrow, C. J. Bond, F. Carniato, M. Botta, M. Braun, Z. Baranyai, R. Pujales-Paradela, M. Regueiro-Figueroa, D. Esteban-Gómez, C. Platas-Iglesias and T. J. Scholl, *Contrast Agents for MRI. Experimental Methods*, ed. V. C. Pierre and M. J. Allen, Royal Society of Chemistry, Croydon, UK, 2017, ch. 3.

44. (*a*) J. R. Lakowicz, *Principles of fluorescence Spectroscopy*, Springer, New York, 3rd edn, 2006, ch. 16; (*b*) P. Bourassa, I. Hasni and H. A. Tajmir-Riahi, *Food Chem.*, 2011, **129**, 1148.

45. (*a*) E. Lissi and E. Abuin, *J. Fluoresc.*, 2011, **21**, 1831; (*b*) D. V. Naik, W. L. Paul, R. M. Threatte and S. G. Schulman, *Anal. Chem.*, 1975, **47**, 267.

46. (*a*) G. Scatchard, *Ann. N. Y. Acad. Sci.*, 1949, **61**, 660; (*b*) T. N. Tikhonova, E. A. Shirshin, G. S. Budylin, V. V. Fadeev and G. P. Petrova, *J. Phys. Chem. B*, 2014, **118**, 6626.

47. K. A. Connors, *Binding Constants. The measurement of molecular complex stability*, John Wiley, USA, 1987, ch. 4 and 12.

48. P. D. Ross and S. Subramanian, *Biochemistry*, 1981, **20**, 3096.

49. L. Alderighi, P. Gans, A. Ienco, D. Peters, A. Sabatini and A. Vacca, *Coord. Chem. Rev.*, 1999, **184**, 311.

50. P. Gans, A. Sabatini and A. Vacca, *Ann. Chim.*, 1999, **89**, 45.

51. D. M. Corsi, C. Platas-Iglesias, H. van Bekkum and J. A. Peters, *Magn. Reson. Chem.*, 2001, **39**, 723.

52. Y. Zhao and D. G. Truhlar, *Theor. Chem. Acc.*, 2008, **120**, 215.

53. F. Weigend and R. Ahlrichs, *Phys. Chem. Chem. Phys.*, 2005, **7**, 3297.

54. M. J. Frisch, G. W. Trucks, H. B. Schlegel, G. E. Scuseria, M. A. Robb, J. R. Cheeseman, G. Scalmani, V. Barone, B. Mennucci, G. A. Petersson, H. Nakatsuji, M. Caricato, X. Li, H. P. Hratchian, A. F. Izmaylov, J. Bloino, G. Zheng, J. L. Sonnenberg, M. Hada, M. Ehara, K. Toyota, R. Fukuda, J. Hasegawa, M. Ishida, T. Nakajima, Y. Honda, O. Kitao, H. Nakai, T. Vreven, J. A. Montgomery, Jr., J. E. Peralta, F. Ogliaro, M. Bearpark, J. J. Heyd, E. Brothers, K. N. Kudin, V. N. Staroverov, R. Kobayashi, J. Normand, K. Raghavachari, A. Rendell, J. C. Burant, S. S. Iyengar, J. Tomasi, M. Cossi, N. Rega, J. M. Millam, M. Klene, J. E. Knox, J. B. Cross, V. Bakken, C. Adamo, J. Jaramillo, R. Gomperts, R. E. Stratmann, O. Yazyev, A. J. Austin, R. Cammi, C. Pomelli, J. W. Ochterski, R. L. Martin, K. Morokuma, V. G. Zakrzewski, G. A. Voth, P. Salvador, J. J. Dannenberg, S. Dapprich, A. D. Daniels, Ö. Farkas, J. B. Foresman, J. V. Ortiz, J. Cioslowski and D. J. Fox, *Gaussian 09*, Gaussian, Inc., Wallingford CT, 2009.

55. J. Tomasi, B. Mennucci and R. Cammi, *Chem. Rev.*, 2005, **105**, 2999.

56. N. Rega, M. Cossi and V. Barone, *J. Chem. Phys.*, 1996, **105**, 11060.

57. E. D. Hedegard, J. Kongsted and S. P. A. Sauer, *J. Chem. Theory Comput.*, 2011, **7**, 4077.

58. P.-A. Malqvist and B. O. Roos, *Chem. Phys. Lett.*, 1989, **155**, 189.

59. (*a*) C. Angeli, R. Cimiraglia and J.-P. Malrieu, *Chem. Phys. Lett.*, 2001, **350**, 297; (*b*) C. Angeli, R. Cimiraglia and J.-P. Malrieu, *J. Chem. Phys.*, 2002, **117**, 9138; (*c*) C. Angeli, R. Cimiraglia, S. Evangelisti, T. Leininger and J.-P. Malrieu, *J. Chem. Phys.*, 2001, **114**, 10252; (*d*) C. Angeli and R. Cimiraglia, *Theor. Chem. Acc.*, 2002, **107**, 313.

60. F. Neese, *Wiley Interdiscip. Rev.: Comput. Mol. Sci.*, 2012, **2**, 73.

61. F. Neese, *J. Chem. Phys.*, 2005, **122**, 034107.

62. A. V. Marenich, C. J. Cramer and D. G. Truhlar, *J. Phys. Chem. B*, 2009, **113**, 6378.

[i] Electronic supplementary information (ESI) available: ^{1}H and ^{13}C NMR spectra of the ligands and their precursors, potentiometric, spectrophotometric and luminescence titrations, optimized Cartesian coordinates obtained with DFT calculations. See DOI: 10.1039/c8dt03856b.